

# One-Shot Clustering for Federated Learning Under Clustering-Agnostic Assumption

**Maciej Krzysztof Zuziak**

*KDD Lab*

*National Research Council of Italy*

*Pisa, PI 56127, Italy*

MACIEJKRZYSZTOF.ZUZIAK@ISTI.CNR.IT

**Roberto Pellungrini**

*KDD Lab*

*Scuola Normale di Pisa*

*Pisa, PI 56126, Italy*

ROBERTO.PELLUNGRINI@SNS.IT

**Salvatore Rinzivillo**

*KDD Lab*

*National Research Council of Italy*

*Pisa, PI 56127, Italy*

RINZIVILLO@ISTI.CNR.IT

## Abstract

Federated Learning (FL) is a widespread and well-adopted paradigm of decentralised learning that allows training one model from multiple sources without the need to transfer data between participating clients directly. Since its inception in 2015, it has been divided into numerous subfields that deal with application-specific issues, such as data heterogeneity or resource allocation. One such sub-field, Clustered Federated Learning (CFL), is dealing with the problem of clustering the population of clients into separate cohorts to deliver personalised models. Although a few remarkable works have been published in this domain, the problem remains largely unexplored, as its basic assumptions and settings differ slightly from those of standard FL. In this work, we present One-Shot Clustered Federated Learning (OCFL), a clustering-agnostic algorithm that can automatically detect the earliest suitable moment for clustering. Our algorithm is based on the computation of the cosine distance between gradients of the clients and a temperature measure that detects when the federated model starts to converge. We empirically evaluate our methodology by testing various one-shot clustering algorithms for over forty different tasks on five benchmark datasets. Our experiments showcase the good performance of our approach when used to perform CFL in an automated manner without the need to adjust hyperparameters. We also revisit the practical feasibility of CFL algorithms based on the gradients or weights of the clients, providing firm evidence of the high efficiency of density-based clustering methods when used to differentiate between the loss surfaces of neural networks trained on different distributions. Moreover, by inspecting the feasibility of local explanations generated with the help of GradCAM, we can provide more insights into the relationship between personalisation and the explainability of local predictions.

**Keywords:** Federated Learning, Clustered Federated Learning, Federated Learning Personalisation, Federated Learning Explainability

## 1 Introduction

The recent decade has witnessed exponential growth in the number of available data sources, primarily due to the expansion of Internet-of-Things (IoT) products and the popularisation of extensive data storing facilities that allow for the storage of unprecedented amounts of information. To leverage such an infrastructure, new paradigms of learning emerge, allowing data engineers and scientists to train models distributively without the need to transfer the data to a central location, which would often be unrealizable due to the sheer volume of stored information.

One such modern approach to decentralised Machine Learning (ML) is FL, a paradigm first introduced by McMahan et al. (2017b) where the local models are trained locally, and the final (global) model is aggregated from the parameters of the local equivalents. Since the baseline FL algorithm has been introduced under the name of Federated Averaging (FedAvg), the field has undergone recent developments with algorithms such as Adaptive Federated Optimisation (FedOpt) (designed by Reddi et al. (2020)), SCAFFOLD (designed by Karimireddy et al. (2020)), and FedProx (designed by Li et al. (2020)) addressing the specifying challenges that may arise in a federated environment.

The task of clustering clients into several conglomerations to train separate (personalised) models is one of such specific challenges that may arise, especially in the cross-silo setting, where the number of participants is limited to dozens rather than thousands and the institutional nature of the participants may require delivery of personalised solutions, at least at the granularity of the regional level. One example of such a situation is training a global risk model for insurance companies, where the significant differences in the local market are so vast that the final (global) model is inoperable for any of the interested parties. In the majority of such situations, companies may not know **(a)** that there exists some form of incongruence and **(b)** what grouping would be required to deliver models of satisfactory quality. The subfield of CFL addresses such issues by applying clustering to the population of clients, delivering several personalised models that still retain some level of generalisability.

In this work, we approach the issue of fast and reliable FL clustering that is automatically performed in the first few rounds of the training. Since many works in the field of CFL employ clustering algorithms on the matrices of pairwise cosine distance (or cosine similarity), our main interest was focused on the generalisation of the presented procedure with an improvement of the clustering efficiency, especially clustering correctness. We, therefore, investigate whether it is possible to automatically detect the suitable clustering moment and perform efficient one-shot clustering at an early stage of the process without specifying any hyperparameters. Moreover, we turned our attention to the scenario of medium heterogeneity, where the clients differ only slightly in data-generating distributions.

We propose a clustering-agnostic algorithm that is free of any hyperparameters and clusters at the first sign of the (global) model’s convergence. Our approach, called OCFL, can be used to perform a reliable clustering in the first rounds of the training without the need to adjust either the number of clusters or the precise clustering criterion. As evidenced by the experimental section, when combined with density-based clustering (e.g., HDBSCAN, designed by Malzer and Baum (2020), or Mean-Shift, designed by Comaniciu and Meer (2002)), it achieves better results than State-of-the-Art CFL algorithms in

terms of clustering performance and personalisation, while retaining comparable levels of generalizability.

In this paper, we hope to contribute to the ongoing discussion by:

1. Presenting a One-Shot Clustering algorithm that extends the previous works published on that topic, especially in the context of empirically proven higher performance and the lack of necessity to fine-tune its hyperparameters;
2. Empirically prove that the cosine distance is an appropriate measure of calculating the differences between federated pseudo-gradients, especially when combined with density-based clustering algorithms, despite claims on the contrary in some positions cited in the literature;
3. Combine the studies on the personalisation measured by local and global performance and the quality of the local explanations. To the best of our knowledge, this work is the first that explore the intersection of local explainability and federated personalisation in clustering.
4. Publish a well-structured code repository that was used for experiments presented in this paper, that can be easily adapted for performing extended experiments in this regard.

The work is heavily oriented towards empirical evaluation of the presented novel algorithms and a better understanding of the impact of personalisation on the local explainability. The area of CFL is still relatively young, and while previous works introduced some theoretical considerations (for example, those presented in Ghosh et al. (2022), Sattler et al. (2021), Mansour et al. (2020), Ruan and Joe-Wong (2022)) as proven in the experimental section of this paper, the empirical evaluations of the State-of-the-Art algorithms not always yields satisfactory results. Part of the problem is the lack of a common methodology for generating data incongruent distributions and empirical evaluation that is limited only to the most popular benchmark datasets. Commencing our work on this paper, we were mainly interested in **(a)** generalisation of the large field of existing methods for CFL that act on gradients of cosine similarity calculated between weights (or gradients) of local models, **(b)** extending the set of those methods by a parameter-free algorithm that superior performance is empirically well-proven and **(c)** incorporating the explainability studies into that framework to advance further our knowledge about the impact of the personalisation on the behaviour of the local networks.

Given our heavy emphasis on an empirical evaluation, we combined standard benchmark datasets (such as MNIST, FMNIST and CIFAR10) with more recent datasets from the medical domain (PathMNIST and BloodMNIST from MedMNIST). Moreover, we opted out of the more trivial data splits, such as label swap, that may render the learning exponentially more difficult, but are straightforward to cluster. Instead, we designed multiple methodologies for overlapping and non-overlapping data silos, where clustering is more challenging but may better reflect the actual situation that occurs under practical circumstances. We also extended the notion of personalisation by examining its impact on local explainability, a concept that, to the best of our knowledge, has not been explored before.

Finally, we aimed to share with the community a well-structured code repository that can be used to redesign our experiments or implement new clustering algorithms. Since our proposition is clustering algorithm agnostic, it can be combined with most of the existing clustering algorithms.<sup>1</sup> All the experiments and their visual representation can be re-created using code deposited at the GitHub Repository shared with this article.<sup>2</sup>

Our paper is organised as follows: in Section 2 we indicate the literature most relevant to our work, in Section 3 we describe in detail our methodology, and in Section 4 we present our experimental evaluation with a detailed discussion on the results. Section 5 is dedicated to experiments related to local explanations generated by clients personalised using certain tested algorithms. Additional considerations for further extending this work are placed under Section 6, while Section 7 contains final conclusions regarding the presented work.

## 2 Related Work

### 2.1 Federated Learning

FL was first introduced in the work of McMahan et al. (2017b) as a decentralised optimisation method, where the training is distributed across several clients and each client shares only the parameters of the model trained on the local data, not disclosing its local (personal) dataset directly. The basic method of solving this problem, FedAvg (presented in McMahan et al. (2017b)) assumes averaging values of the local parameters to arrive at the general global model. In the following years, different additional solutions to that problem were presented. Federated Optimisation (FedOpt) (introduced by Reddi et al. (2020)) generalises the FedAvg algorithm, allowing one to introduce adaptive optimisation into the process. Among others, SCAFFOLD (designed by Karimireddy et al. (2020)) and FedProx (designed by Li et al. (2020)) tackle the issue of data heterogeneity, limiting the gradient variability and thus stabilising the convergence process. As FL became an important area of research, several surveys have tried to summarise the advancements made in the last decade of research, such as those presented by Kairouz et al. (2021) or Wang et al. (2021). In this paper, we assume a horizontal learning scenario. In contrast to the vertical setting (surveyed, for example, by Liu et al. (2024)), the horizontal one assumes that the sample space is disjoint, while the feature space is shared among all the participants. Implementing our clustering algorithms, we employ a FedOpt baseline. Given a set of disjoint datasets  $D = \bigcup_{i \in P} D_i$ , where each dataset  $D_i = \{\mathbf{x}_i, y_i\}_{i=1}^k$  is generated according to a certain probability distribution, i.e.  $D_i \sim \varphi_i$ , the FL task is to optimize global hypothesis function using aggregation of the locally trained functions, i.e.  $\operatorname{argmin}_{h \in \mathcal{H}} R_{ERF}(h, D) \approx \frac{1}{|P|} \operatorname{argmin}_{h \in \mathcal{H}} R_{ERF}(h, D_i)$ , where  $P$  is the size of the population. In order to do that, we employ the FedOpt algorithm presented in Reddi et al. (2020), which is a well-accepted baseline.

### 2.2 Clustering in FL

Clustering is one of the approaches to personalisation in FL. Mansour et al. (2020) distinguishes it as one of the three key methods, along with the model and data interpola-

---

1. The GitHub repository with the code base for performing simulation can be found under the following link.  
 2. The GitHub repository with all the relevant numerical results and code for generating plots.

tion, while the survey of Tan et al. (2023) places it under the umbrella of similarity-based approaches. We observe that CFL is currently predominantly divided into two distinct approaches, which we call here *hypothesis-based clustering* and *parameters-based clustering*. The primer is based on the similarity of the hypothesis function (such as methods presented by Ghosh et al. (2022) and Mansour et al. (2020)) and relies on matching clients with the most similar objective functions. The former relies on the similarity of the local models’ parameters, as they can disclose information about the local data-generating process (this paradigm is reflected in the works of Briggs et al. (2020), Sattler et al. (2021) Duan et al. (2021), Gong et al. (2022b) Palihawadana et al. (2022) and Tian et al. (2022)). In this paper, we take a closer look at the second group of methods as we propose a natural extension of methods based on the similarity between the local sets of parameters.

Much of the work in the *parameters-based clustering* domain relies on comparing weights or gradients provided by the local models. Two main aspects that distinguish particular approaches are the time of the clustering and the clustering algorithm. Briggs et al. (2020) proposes using hierarchical clustering based on models’ parameters. Their work implies fixing a clustering round *a priori* together with a choice of a proper linkage criterion and its corresponding hyperparameters (mainly, distance threshold). The work of Sattler et al. (2021) relies on a cosine similarity-based bipartitioning, where the clustering is based on the cosine similarity between different sets of parameters. Since the clustering is postponed until the (global) FL model converges to a stationary point, it is deemed a postprocessing method. The work of Duan et al. (2021) employs an Euclidean distance of Decomposed Cosine Similarity (EDC) to cluster clients. Gong et al. (2022a) mixes distance comparison with client-side adaptation (varying number of local epochs) and weighted voting. Palihawadana et al. (2022) uses pairwise similarity to measure the statistical heterogeneity of the local datasets. Tian et al. (2022) experiments with the use of cosine distance and client-side code execution to correct possible erroneous clustering results (by individual client drop-out).

Our work resembles propositions made by Sattler et al. (2021) and Briggs et al. (2020). Hence, those two articles serve as our natural point of comparison. By experimenting with different types of splits (with a heavier emphasis on the *feature skew* and *label skew*), we hope to further expand their methods in a more challenging (clustering-wise) environment and automatically identify the earliest possible moment for performing one-shot clustering. Because our method falls within the *parameters-based clustering*, it can also serve as a possible augmentation for methods presented by Duan et al. (2021), Gong et al. (2022a), Tian et al. (2022) and Palihawadana et al. (2022).

Our work assumes comparing the complete parametrisation of the neural networks, not their lower-dimensional representation, as in the case of - for example - Duan et al. (2021). The reason for that is the basic assumption underlying our method, that it should be, in principle, clustering algorithm agnostic. Moreover, as evidenced by the numerous experiments reported in this paper, density-based clustering algorithms such as HDBSCAN (introduced by Malzer and Baum (2020)) or Mean Shift (introduced by Comaniciu and Meer (2002)) are unexpectedly efficient when dealing with a complex parametrisation of the State-of-the-Art neural networks. Moreover, in contrast to works of Ruan and Joe-Wong (2022) and Li et al. (2022), we assume a **hard clustering** problem, where we want to detect the existence of a disjoint and well-defined clustering structure within the trained population.

Those two assumptions are crucial for defining our baseline comparison benchmarks, so those of Sattler et al. (2021) and Briggs et al. (2020).

### 3 Methodology

#### 3.1 Data Generating Processes

##### 3.1.1 THEORETICAL INCONGRUENCE IN TARGET POPULATION

Simulating a divergence in data-generating processes that resembles the naturally occurring differences in data distributions is a challenge that is approached in various ways. Tian et al. (2022) and Gong et al. (2022a) adopt label distribution and dataset distribution skew, with Tian et al. (2022) additionally experimenting with differences in feature distribution. Both Sattler et al. (2021) and Briggs et al. (2020) employ label swaps to stimulate incongruence in data distribution. Ma et al. (2022) follows the methodology presented by McMahan et al. (2017a) using the Dirichlet distribution to simulate a heterogeneous environment. Additionally, FEMNIST (employed by Briggs et al. (2020) and Palihawadana et al. (2022)) and Fed-Goodreads (employed by Palihawadana et al. (2022)) are employed in some papers.

Considering that there is no consensus on how to simulate naturally occurring clusters of users in FL, we have adopted a precise methodology focused on the data-generating processes that could potentially arise in a natural environment. This formalisation allows us to develop various complicated scenarios while retaining a firm methodology for generating the data splits. Firstly, the existence of various data-generating processes is assumed. Those processes (framed as stochastic functions) are formally defined in Definition 1

**Definition 1 (Data Generating Process (DGP))** *Let  $\Omega$  define a sample space and let  $\mathcal{X} = \mathbb{R}^d \times \mathcal{Y}$  where additionally  $\mathcal{Y}$  is assumed to be finite. The  $\zeta_i$  is a stochastic function associated with a certain cluster  $c_i$ . Then:*

$$D_k = \{(x_j, y_j) \sim \zeta\}_{j=0}^n \quad (1)$$

*is a dataset of length  $n$  generated by this process. Similarly, using a push-forward measure notation, let  $\mathbb{P}$  define a pushforward measure under  $\zeta_i$  and let  $P^{(i)} = \mathbb{P} \circ \zeta_i^{-1}$  denote the induced distribution. Then, for any measurable set  $A \in \mathcal{A}$ ,*

$$D_k = \mathbb{P} \circ \zeta_i^{-1} \quad (2)$$

Let us further assume that there exists a possibly infinite set of data-generating processes  $\zeta$  that for each  $\zeta_i \in \zeta$ . The goal of the CFL task is to assign clients to clusters according to their original data generation mechanism. In the presented setting, this is reflected on the cluster level, where the population of clusters  $C = \{c_1, c_2, \dots, c_n\}$  is attributed to individual data-generating distributions by an injective non-surjective function  $\mathcal{I} : C \rightarrow \zeta$ , *i.e.*, each cluster corresponds to at most one data-generating distribution, but some data-generating distributions will not be attributed to any cluster at all. The client-cluster correspondence is established by a non-injective surjective function  $\mathcal{Z} : P \rightarrow C$ , *i.e.*, each client is attributed

to some cluster with clusters grouping possibly more than one client.<sup>3</sup> The notion of DGP-Cluster mapping is formalised in Definition 2.

**Definition 2 (DGP - Cluster Mapping)** *Let  $\zeta$  be an infinite set of all possible data-generating processes, such that each  $\zeta_i \in \zeta$ , and let  $C = \{c_i\}_{i=0}^d$  be a finite set of clusters. Then, each cluster will be uniquely attributed a certain data-generating process by an injective, non-surjective function:*

$$\mathcal{I} : C \longrightarrow \zeta \quad (3)$$

*which implies that  $\mathcal{I}(c_i) = \zeta_i \quad \forall \zeta \in \Phi$ . Furthermore, let  $P = \{p_i\}_{i=0}^m$  be a population of clients. Then, the client mapping is defined uniquely by a surjective non-injective function:*

$$\mathcal{Z} : P \longrightarrow C \quad (4)$$

*which implies that  $\mathcal{Z}(p_i) = c_i \quad \forall p_i \in C$*

The Definition 1 and 2 allows for expressing a clustering scenario rigidly in a federated setting. However, in practice, the data-generating process is reflected by a choice of a proper probability distribution. For example, if the dataset  $D = \{\mathbf{x}_i\}_{i=1}^n$  is created by repeatedly sampling from a  $k$ -dimensional vector  $\mathbf{x}$  from a multivariate normal distribution parametrised by a mean-vector  $\boldsymbol{\mu}$  and covariance matrix  $\boldsymbol{\Sigma}$ , one would write  $D \sim \mathcal{N}(\boldsymbol{\mu}, \boldsymbol{\Sigma})$ . Using this notation, we introduce the method of simulating naturally occurring clusters by sampling from multiple probability distributions that should reflect a finite number of data generating processes  $\Phi = \{\varphi_1, \varphi_2, \dots, \varphi_n\}$ , where each local dataset is either sampled from the probability distribution  $\mathcal{D}_k \sim \varphi_i[\mathbf{x}]$  or is based on the conditional probability distribution  $\mathcal{D}_k \sim \varphi_k[\mathbf{x}|\mathbf{y}]$ .

### 3.1.2 PRACTICAL SIMULATION OF CLUSTERED POPULATION

In practice, one would preferably opt for a standard benchmarking dataset as a point of validation for the tested algorithms. To simulate various levels of divergence, while still being consistent with the methodology presented above, we define two different split scenarios: **(i) overlapping** and **(ii) non-overlapping** splits. **Non-overlapping** simulates a behaviour encountered in data silos when the set of classes is completely disjoint from the set of classes available in the different silo. **Overlapping** is more challenging clustering-wise, as it implies that there is some overlap between those two sets. It may be caused, for example, by the fact that both distributions are part of the same parametric family, but the respective parameters are not identical.

Formally, given a set of label occurring in the population  $\mathcal{Y} = \{\mathcal{Y}_n\}_{n=1}^k$ , we define a set of disjoint label subspaces, *i.e.*,  $\hat{\mathcal{Y}} = \{\mathcal{Y}^c \subset \mathcal{Y} | c \in C\}$ . The union of the non-overlapping subspaces is an empty set, *i.e.*,  $\bigcap_{c \in C} \mathcal{Y}^c = \emptyset$ . Conversely, the union of an overlapping subspaces will not be empty, *i.e.*,  $\bigcap_{c \in C} \mathcal{Y}^c \neq \emptyset$ .

The following provides information about the overlap in the label space  $\mathcal{Y}$ , but tells nothing about the actual probability distributions assigned to each cluster. This is controlled

---

3. Alternatively, split the population of clients into the subsets  $\hat{p}_i$  such that  $P = \bigcup_{i=0}^n \hat{p}_i$  and there exists a surjective non-injective function mapping clients to subsets. Additionally, ensure that  $|\hat{P}| = |C|$ . Then, the mapping can be expressed by a bijective function  $\mathcal{T} : C \longrightarrow \hat{P}$

by introducing further sub-splits, in the form of **(i) balanced (homogeneous)** and **(ii) imbalanced (heterogeneous)** settings. To simulate that, firstly the distribution across labels is fixed, *i.e.*,  $\mathbf{y}_c \sim \varphi_c$  and then the features are drawn from a conditional distribution  $\mathbf{x} \sim \varphi(\mathbf{x}|\mathbf{y}_c)$ , with this exception, that the  $c$  denotes the  $c^{th}$  cluster, not individual clients.

For the **balanced scenario**, each cluster follows a uniform distribution across classes allocated to it, *i.e.*,  $\mathbf{y}_n^c \sim \text{Unif}(\mathcal{Y}^c)$  and  $\mathbf{x} \sim \varphi_c(\mathbf{x}|\mathbf{y}_n^c)$ , where  $c$  is the  $c^{th}$  cluster and  $n$  is the  $n^{th}$  class. For the imbalanced split, for each cluster  $c \in C$ , a class distribution vector  $\mathbf{v}^c \sim \text{Dir}(\boldsymbol{\alpha})$  is generated, where  $\boldsymbol{\alpha} = \alpha * \mathbb{1}_k$  is a symmetric Dirichlet prior. Afterwards, the distribution of a particular class is defined by a Categorical distribution with a parameter  $\bar{\mathbf{v}}^c$ , *i.e.*,  $\mathbf{y}_n^c \sim \text{Categorical}(\bar{\mathbf{v}}^c)$  and the data points are drawn accordingly,  $\mathbf{x} \sim \varphi(\mathbf{x}|\mathbf{y}_n^c)$ , where  $c$  denotes the  $c^{th}$  cluster and  $n$  denotes the  $n^{th}$  class. We model the prior distribution  $\varphi(\mathbf{y})$ , while the posterior distribution  $\varphi(\mathbf{x}|\mathbf{y})$  is encoded by the dataset itself. The method of defining a Dirichlet distribution over a set of available labels is widely accepted in the research on Federated Optimisation (see Reddi et al. (2021)) and Federated Clustering (see Wei et al. (2020)).

On the final note, we disclose that we employ a light re-sampling schema that allows one data point to be shared between two or more clients. We motivate this approach by highlighting the first part of the non-i.i.d. (non-independent and identically distributed) phrase, which is always invoked in the federated setting but is seldom realised in the experimental environment. The lack of independence is often overlooked when creating the data splits, especially when the experimental data does not consist of a time series. Hence, we have tried to simulate an environment one a particular data point may be shared across the clients of the same cluster or even belonging to clients from different clusters, hence violating the assumption of independence and making clustering more challenging.

When compared with the taxonomy of non-identical client distributions presented by Kairouz et al. (2021), the presented methodology allows for a rigid expression of a *feature distribution skew* (where  $\varphi_i[\mathbf{x}]$  vary across clients, with  $\varphi_i[\mathbf{y}|\mathbf{x}] = \varphi_j[\mathbf{y}|\mathbf{x}] \quad \forall i, j \in P$ ) and *label distribution skew* (where  $\varphi_i[\mathbf{y}]$  vary across clients, with  $\varphi_i[\mathbf{x}|\mathbf{y}] = \varphi_j[\mathbf{x}|\mathbf{y}] \quad \forall i, j \in P$ ), additionally combined with *quality skew* and the non-independence of the feature and label space (shared examples). We do not consider *concept drift* and *concept shift* in this paper. While important for studying the effect of convergence in highly heterogeneous environments, feature and label distributions are the most difficult to capture because the model may differ subtly while still benefiting from clustering. On the other hand, it is implied that the case of extreme heterogeneity impacts learning to the utmost level, hence being easier to detect - a fact proven by previous authors published on the topic, such as Briggs et al. (2020), Ghosh et al. (2022), Sattler et al. (2021).

### 3.2 Hypothesis Function Similarity

Accessing the information about the local distribution is impossible, as it would nullify the basic assumption underlying the FL. However, some information about the status of the learning can be derived from the model's parameters that reflect a local hypothesis function. For each cluster  $C_i \in C$ , there exists a hypothesis function  $h_{C_i}$  that minimizes the empirical risk function on a dataset sampled from the corresponding data-generating distribution, *i.e.*  $h_{C_i}^* = \argmin_{h \in \mathcal{H}} R_{ERF}(h, D_i)$ , where  $D_i \sim \varphi_i$ . Every client belonging to a certain cluster



is training their own hypothesis function  $h_{p_i}$  that minimises the local risk function. The hypothesis function  $h_{C_i}^*$  is not guaranteed to outperform the local hypothesis function  $h_{p_i}$  in every case since it depends on the data stored on the local client. However, given the environment,  $h_{C_i}^*$  will be the function that minimises the empirical risk for the whole cluster. One illustrative example may be connected to a small sample size of the local dataset. If the client is in possession of only a few samples, an overfitted local hypothesis function may outperform the best cluster hypothesis function. However, as the client will procure new samples, the best cluster hypothesis function will perform better than the overfitted local function. Those notions are formalised in the Definition 3.

**Definition 3 (Cluster Hypothesis Function)** *The **Cluster Hypothesis Function** is a hypothesis function from a family of hypothesis functions  $h \in H$  that minimises the empirical risk on average on all clients belonging to a certain cluster, i.e.,*

$$\operatorname{argmin}_{\Theta \in \Theta} \mathbb{E}[R_{ERF}(x_{i \sim \varphi_i}, y_{i \sim \varphi_i}, \Theta_i)] \quad (5)$$

The similarities of local loss functions are used by Ghosh et al. (2022) or Mansour et al. (2020) to cluster the population of clients into a predefined number of clusters. This approach suffers from a high computational cost (as each client must test out each possible hypothesis function to find the one that minimises the local risk) and the necessity to know *a priori* the structure of the population, i.e., the number of total clusters. However, one could note that the hypothesis function  $h_i$  is parameterised by the  $n$ -dimensional tensor  $\Theta$ .<sup>4</sup> The flattened one-dimensional version of this tensor, i.e.  $\hat{\Theta} = \operatorname{Vec}(\Theta)$ , can be compared with other parameterised hypothesis functions without the need to directly assess the hypothesis function performance on the local dataset - the method used in Briggs et al. (2020), Duan et al. (2021), Sattler et al. (2021) or Tian et al. (2022).

The current state of the art does not provide answers to when the clustering could be initialised at the earliest. To develop an intuitive understanding of the problem, let  $C_s(\hat{\Theta}_i, \hat{\Theta}_j)$  denote **cosine similarity** between vectors of parameters  $\hat{\Theta}_i$  and  $\hat{\Theta}_j$  and  $C_d(\hat{\Theta}_i, \hat{\Theta}_j) = 1 - C_s(\hat{\Theta}_i, \hat{\Theta}_j)$  denote a **cosine distance**. Those are placed in Definitions 4 and 5 for reference.

**Definition 4 (Cosine Similarity)**

$$C_s(\hat{\Theta}_i, \hat{\Theta}_j) = \frac{\hat{\Theta}_i \times \hat{\Theta}_j}{\|\hat{\Theta}_i\| \|\hat{\Theta}_j\|} = \frac{\sum_k^n \hat{\theta}_{k(i)} \hat{\theta}_{k(j)}}{\sqrt{\sum_i^n \hat{\theta}_{k(i)}^2} \sqrt{\sum_i^n \hat{\theta}_{k(j)}^2}} \quad (6)$$

and  $C_s(\hat{\Theta}_i, \hat{\Theta}_j) \in [-1, 1]$ .

---

4. The dimensions of the tensor will depend on the used model. In the case of conventional  $n$  layered feedforward neural networks, the weights are often represented in  $n - 1$  separate matrices of size  $a \times b$ , where  $b$  is the number of neurons in the layer  $j$  and  $a$  is the corresponding number of neurons in the  $j + 1$  layer. This can be represented as a three-dimensional tensor  $\Theta \in \mathcal{R}^{n-1} \times \mathcal{R}^a \times \mathcal{R}^b$ . Without the loss of generality, we assume that  $\Theta \in \mathcal{R}^n$  or  $\Theta \in \mathcal{R}^n \times \mathcal{R}^m$  where  $n, m \in \mathbb{Z}$ .

**Definition 5 (Cosine Distance)**

$$C_d(\hat{\Theta}_i, \hat{\Theta}_j) = 1 - C_s(\hat{\Theta}_i, \hat{\Theta}_j) = 1 - \frac{\hat{\Theta}_i \times \hat{\Theta}_j}{\|\hat{\Theta}_i\| \|\hat{\Theta}_j\|} \quad (7)$$

and  $C_d(\hat{\Theta}_i, \hat{\Theta}_j) \in [0, 2]$ .

Subsequently, define  $\mathbf{\Gamma} \in \mathcal{R}^{m \times m}$  symmetric matrix that captures the similarity between the parametrisation of a hypothesis function provided by all the sampled clients. The  $(i, j)$  entry of this matrix will be defined as  $\gamma_{(i,j)} = \gamma_{(j,i)} = C_d(\hat{\Theta}_i, \hat{\Theta}_j)$  and the whole matrix will be called Divergence Matrix as in Definition 6.

**Definition 6 (Divergence Matrix)** Let  $\Theta = \{\hat{\Theta}_i\}_{i=0}^n$  denote the set of individual parametrisations dispatched by clients. Then, the **Divergence Matrix**  $\Theta \in \mathbb{R}^{n \times n}$  is a symmetric matrix s.t.:

$$\Gamma_{(i,j)} = \Gamma_{(j,i)} = C_d(\hat{\Theta}_i, \hat{\Theta}_j) = 1 - C_s(\hat{\Theta}_i, \hat{\Theta}_j) = 1 - \frac{\hat{\Theta}_i \times \hat{\Theta}_j}{\|\hat{\Theta}_i\| \|\hat{\Theta}_j\|} \quad (8)$$

Matrix  $\mathbf{\Gamma}$  captures the learning divergence between the sampled nodes. To obtain a single-valued description of the current convergence progress, we define the **Clustering Temperature Function** in Definition 7.

**Definition 7 (Temperature Function with Norm  $p$ )** Let  $\Theta \in \mathbb{R}^{n \times n}$  be a Divergence Matrix (Definition 6). Then, the **Clustering Temperature Function with Norm  $p$**  is defined as:

$$T(\mathbf{\Gamma}) = \frac{\|\mathbf{\Gamma}\|_p}{\lambda} \quad (9)$$

where additionally  $\lambda > 0$  and  $p$  is a chosen norm s.t.:

$$\|\mathbf{\Gamma}\|_p = \|\text{vec}(\mathbf{\Gamma})\|_p = \left( \sum_{i=1}^m \sum_{j=1}^n |\gamma_{i,j}|^p \right)^{\frac{1}{p}} \quad (10)$$

This implies that the definition of temperature introduced here will be based on the  $p$ -norm of the **Divergence Matrix** from Definition 6 and scaled by a certain constant  $\lambda$ . It should be observed, that if the  $\mathbf{\Gamma}$  is  $n \times n$  square matrix, then  $0 \leq \|\mathbf{\Gamma}\|_p \leq \sqrt[p]{n(n-1)2^p}$ . This is a **Maximal Divergence Constant** that we will use throughout this work. However, since cosine distance is always non-negative, we can also define  $\lambda = \frac{1}{\Gamma_{max}}$  as a **Normalising Constant**. The important highlight here is that one should not observe as much the absolute value of the Temperature Function defined in Definition 7, but its relative value with respect to previous rounds, i.e.  $\Delta T(\mathbf{\Gamma})$ .

**3.3 Clustering Procedure**

The proposed algorithm is based on the empirical observations of the **Temperature Function** from Definition 7. The preliminary hypothesis assumed that the function  $T$  may express two different types of behaviours: (i) either the value may decrease at the beginning

of the training (initial convergence) and then rise after reaching a local minimum due to incongruence of the data splits, or **(ii)** it may rise from the very beginning without reaching a local minimum at all due to aforementioned incongruence of the data splits. Those preliminary assumptions were verified with the detailed and repeated observation of the **Temperature Function** behaviour over multiple datasets and multiple data splits (this is evidenced and discussed in the Subsection 4.5).

Using this observation, we present an ***One-Shot Clustered Federated Learning (OCFL)*** in Algorithm 1. Following this procedure, the first initial cluster is equal to the whole population.<sup>5</sup> The first  $T_{-1}$  value is set to *inf* (line 6). As mentioned earlier, two types of behaviours are expected: we either **(i)** observe a descent and wait for the first sign of a rise or **(ii)** await the rise of the gradients from the very beginning of the training. Since we are considering one-shot clustering, the flag  $\mathcal{F}$  is initially set to false (line 7). Lines 8-14 describe the beginning of the standard FL process, with computation of local stochastic gradient (line 12), performing local update (line 13) and computing local model delta (line 14), all done in parallel. After the gradients are aggregated, the next step is to check whether the clustering was already performed (line 15). If not, the matrix  $\Gamma$  capturing the cosine distance between the gradients is reconstructed, and the **Clustering Temperature** (Definition 7) is calculated (line 16-19). If the newly registered temperature exceeds the one previously registered (line 20), the algorithm performs an actual clustering and switches the flag  $\mathcal{F}$  to *True*. Otherwise, it simply returns the initial clustering structure (line 25). The in-cluster models are reconstructed from gradients of clients attributed to a specific cluster (lines 26-28). Please note that for clarity, a symbol of  $\Theta$  was replaced with a symbol  $\theta$  in the description of the algorithm.

## 4 Experiments

In this section, we present a number of experiments evaluating the performance of OCFL algorithm (Subsection 4.3), the impact of the clustering on the personalization (performance on the local test set) and generalisation (performance on the hold-out test set) (Subsection 4.4) and the behaviour of the *Clustering Temperature* Function (Subsection 4.5). The data on which the tests were evaluated is reported at the beginning of this section (Subsection 4.1), and the experimental setting is reported in Subsection 4.2. The experimental work related to cluster-level explainability is presented in a separate section (Section 5).

### 4.1 Datasets

We experiment on five different image classification datasets with increased levels of difficulty: MNIST (LeCun and Cortes (2010)), FMNIST (Xiao et al. (2017)), CIFAR10 (Krizhevsky (2009)), PATHMNIST and BLOODMNIST (Yang et al. (2023)). We use the methodology described in subsection 3.1 to simulate four different types of data splits: **(i)** overlapping balanced, **(ii)** non-overlapping balanced, **(iii)** overlapping imbalanced and **(iv)** non-overlapping imbalanced for **(a)** 15 and **(b)** 30 clients. The combination of five datasets,

---

5. The presented algorithm assumes sampling the whole population each round. However, a dynamic environment (where clients appear and disappear on an ongoing basis) can be taken into consideration in several different ways. This is explored in additional research directions at the end of this paper.

---

**Algorithm 1:** One-Shot Clustered Federated Learning (OCFL)

---

```

1 input ServerOpt
2 input ClientOpt
3 input  $\eta_c, \eta_s$  Learning Rates
4 input  $\mathcal{A}(\cdot)$ , Clustering Algorithm
5 input  $C = \{P\}$ , Set of Clusters
6  $T_{-1} \leftarrow \inf$ 
7  $\mathcal{F} \leftarrow False$ 
8 for  $t = 0, \dots, T$  do
9   for client  $i \in P$  in parallel do
10     $\theta_i^{(t,0)} \leftarrow \theta^t$ 
11    for  $k = 0, \dots, K$  do
12       $g_i(\theta_i^{(t,k)}) \leftarrow \nabla \mathcal{L}(h(D_i, \theta_i^{(t,k)}), y)$ 
13       $\theta_i^{(t,k+1)} = \text{ClientOpt}(\theta_i^{(t,k)}, g_i(\theta_i^{(t,k)}), \tau)$ 
14     $\Delta_i^{(t)} \leftarrow \theta_i^{(t,K+1)} - \theta_i^{(t,0)}$ 
15  if  $\mathcal{F} == False$  then
16     $\Gamma^{(t)} \leftarrow C_d(\Delta^{(t)})$ 
17     $\lambda \leftarrow \sqrt[p]{n(n-1)2^p}$ 
18     $T_{t-1} \leftarrow T_t$ 
19     $T_t \leftarrow \frac{\|\Gamma^{(t)}\|_p}{\lambda}$ 
20    if  $T_t \geq T_{t-1}$ 
21      then
22         $C \leftarrow \mathcal{A}(\Gamma)$ 
23         $\mathcal{F} \leftarrow True$ 
24      else
25         $C \leftarrow C$ 
26  for  $C_j \in C$  do
27     $\Delta_j^{(t)} \leftarrow \{\Delta_i^t | i \in C_j\}$ 
28     $g_{C_j} = \frac{1}{|C_j|} \sum_{k \in \Delta_j^t} \Delta_K^t$ 

```

---

four different splits, and two client cardinalities provides for a total of 40 different scenarios. Given seven different algorithms to test, this implies 280 separate runs.

The theoretical assumptions regarding the data splits were presented in Subsection 2. The **non-overlapping balanced splits** resemble the most basic case, where the cluster has access to separate classes, the agents are uniformly distributed across the clusters (with the same number of agents belonging to each cluster), and the available labels are uniformly distributed across the clients. The **overlapping balanced split** implies similar circumstances but with a partial overlap of classes, i.e., the clients partially share some of the classes. Imbalance is simulated across two different levels simultaneously. Firstly, clients are unevenly distributed across clusters. The first cluster holds 20% of the clients, while the second and third are approximately 47% and 33%, respectively. Secondly, the prior distribution across labels is not uniform but is sampled according to a weight vector  $\sim \text{Dir}(\bar{v})$ , where  $\bar{v}$  is defined as before. The **non-overlapping imbalanced split** assumes that the data is distributed according to  $\text{Dir}(\bar{v})$ , but the set of classes is still disjoint across the clusters. Prior Subsection 3 contains all the relevant information regarding the rigid methodology for performing the splits.

## 4.2 Experimental Set-up

Given that our proposal is clustering algorithm-agnostic, we combine it with density-based clustering methods, such as Mean Shift (proposed by Malzer and Baum (2020)) and HDBSCAN (proposed by Comaniciu and Meer (2002)), or parameter-free methods, such as Affinity Propagation (introduced by Frey and Dueck (2007)). We employ four different baselines to test out the algorithm’s general capabilities. The first one is **Baseline No-Clustering (BNC)**, which implies keeping all the clients in one cohort, as is done in vanilla FL. The next two baselines are derived from the literature, namely **Clustered Federated Learning: Model-Agnostic Distributed Multitask Optimisation Under Privacy Constraints (SCL)** developed by Sattler et al. (2021) and **Federated Learning with Hierarchical Clustering of Local Updates to Improve Training on Non-IID Data (BCL)** presented by Briggs et al. (2020). The fourth baseline measures the performance of our algorithm in an ideal state, that is, a combination of **OCFL with K-Means (OCFL-KM)** where the number of data-generating distributions is known *a priori*. Those four baselines are then compared against the combination of OCFL with HDBSCAN (**OCFL-HDBS**), Mean-shift (**OCFL-MS**) and Affinity Propagation (**OCFL-AFF**). The following section presents the experiments carried out to assess their efficiency in comparison to other algorithms.

To solve the MNIST and FMNIST tasks locally, we employ a Deep Convolutional Neural Network of our architecture, inspired by Tiny-VGG as presented by Simonyan and Zisserman (2015). To solve CIFAR10, PathMNIST and BloodMNIST tasks, we employ the ResNet34 architecture in the form introduced by He et al. (2016). According to the experiments performed on the centralised version of the datasets, we were able to achieve a 99% and 94% test accuracy on MNIST and FMNIST tasks, respectively, and around 82% of accuracy on the CIFAR10 test set. Similarly, in a centralised setting of the PathMNIST and BloodMNIST dataset, ResNet34 obtained a result comparable to the State-of-the-Art reported by Yang et al. (2023). To rule out the possibility that excessive hyperparameter

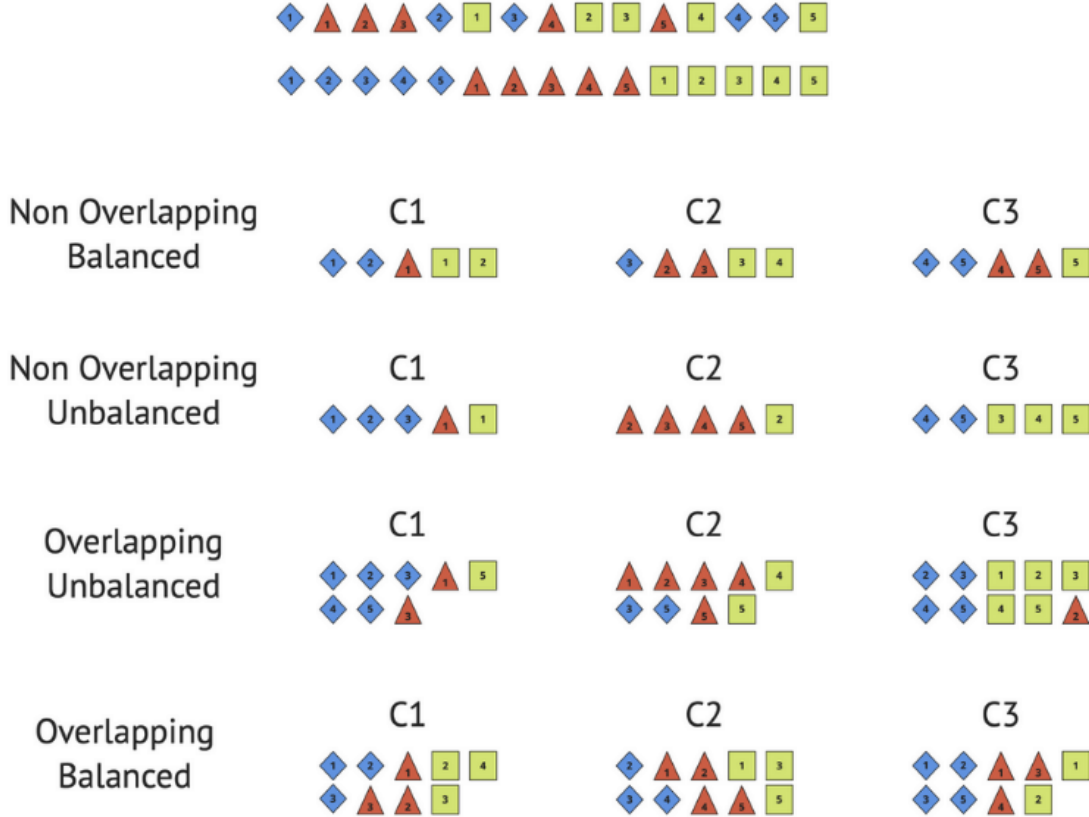


Figure 1: Visualisation of different data distributions in CFL. The different shapes represent different classes, while the integers imprinted into them serve as local identifiers. Four different splits are presented in each row, where each individual column is a separate cluster. As indicated by the individual numbers displayed on the shapes, some particular samples may be shared between the clusters.

fine-tuning influences the clustering results, Stochastic Gradient Descent (SGD) was employed, and a shared local learning rate of 0.01 was used for solving the MNIST, FMNIST, and CIFAR10 tasks. For MNIST and FMNIST batch size was set to 32 samples, while for CIFAR10, it was set to 64 samples. Only for PathMNIST, an Adam Optimiser (introduced by Kingma and Ba (2015)) was selected with a learning rate of  $1e - 7$ , batch size equal to 128 samples and weight decay of 0.01. This was done to ensure a smooth convergence of the learning process. The same was done for the BloodMNIST, where the Adam Optimiser was chosen with a learning rate of  $1e - 6$ , batch size equal to 128 samples and weight decay of 0.01. This is summarised in Table 3 in the Appendix to this work.

We employ a baseline FedOpt algorithm described in Section 2.1 for the Federated Learning part. While the method can be easily adapted to other algorithms described in that section, FedOpt (that is, a generalisation of FedAvg) can serve as a stable and easy-to-compare baseline. In our library, we have implemented algorithms of Briggs et al. (2020) and Sattler et al. (2021) from scratch, using pseudo-algorithms provided in their papers as well as publicly available code in the case of Sattler et al. (2021).<sup>6</sup> Since the original implementation included in the GitHub repository contained an additional hyperparameter - a minimal number of rounds after which clustering can be performed - we have also transferred that hyperparameter into our library. Given that the algorithm of Sattler et al. (2021) requires three hyperparameters (including the cool-down period, which is incorporated in the code presented on GitHub), the original authors’ recommendations were employed to select a set of optimal hyperparameters for a fair comparison. One problem that is connected to that is that authors recommend setting the values of epsilons as  $\epsilon_1 = \max_t \|\Delta\theta_c^t\|/10$  and  $\epsilon_2 \in [\epsilon_1, 10\epsilon_1]$  where  $\Delta\theta_i^t = \text{SGD}(\theta^{t-1}, D_i) - \theta^{t-1}$ . This would require running all the simulation splits, registering the magnitude of gradients, observing the maximal possible magnitude and then choosing that value as a hyperparameter for another run, while also adjusting the cool-down round that was mentioned before. Given the number of simulations performed for the presented studies, this would yield a highly impractical workflow. Moreover, we have noticed that in the original implementation placed in the GitHub repository, Sattler et al. (2021) also does not construct their experiments in such a way, providing specified  $\epsilon_1$  and  $\epsilon_2$  values from the beginning. Because of that, an approximation method was constructed for both values. We have performed a centralised training on an original dataset and defined a proxy value  $\Delta\hat{\theta}^t = |\text{SGD}(\theta^t, D) - \text{SGD}(\theta^{t-1}, D)|$  that is used in exchange for the original  $\theta$  value. Afterwards, the round of convergence is used to select the value for a cool-down period. The recommendations from Sattler et al. (2021) are used to select values of  $\epsilon_1$  and  $\epsilon_2$ . If that failed, we turned to a heuristic search based on the code made available by the authors. In that way, it was established that one workable combination for MNIST and FMNIST datasets is  $\epsilon_1 = 0.35$  and  $\epsilon_2 = 1.00$ . No such combination was found for CIFAR-10 and PathMNIST or BloodMNIST datasets. For the algorithm reported by Briggs et al. (2020), we experimented with a distance threshold in the  $[0.05, 0.4]$  range, cosine similarity metric and linkage by averaging. Only the best average results were kept.

For each split of the dataset, we run 50 (MNIST, FMNIST), 75 (PathMNIST and BloodMNIST) or 80 (CIFAR-10) global training rounds, where three local epochs precede one round. Since the HDBSCAN requires a minimal cluster size and we wanted to keep our

6. The code used for re-implementation of the work of Sattler et al. (2021) can be found under the following link.

clustering method hyperparameter-free, the minimal cluster size is always set to 20% of the sample size.

### 4.3 Clustering Evaluation

We evaluate clustering by measuring the ability of the algorithm to attribute each client to its data-generating cluster correctly. Since the presented notion of CFL is wholly based on the number of pre-defined data-clustering distributions (as described in Subsection 3.1), we can test out the performance of an original bijective function  $\mathcal{T} : C \rightarrow \mathcal{P}$ , attributing a subset of clients to a certain cluster and the returned function  $\hat{\mathcal{T}}$ . Given the population  $P = \{p_1, p_2, p_3, \dots, p_n\}$ , we can define the original partition of  $P$  into  $n$  clusters, i.e.  $C = \{C_1, C_2, \dots, C_n\}$  and the automatically detected partition of  $P$  into  $n$  subsets, i.e.  $\hat{C} = \{\hat{C}_1, \hat{C}_2, \dots, \hat{C}_m\}$ . The closer the former resembles the primer, the better the formal clustering correctness of the presented solution. To evaluate the presented clustering methods, we employ **Rand Index (RAND)**, **Adjusted Mutual Information (AMI)** and **Completeness Score (COM)**.

The method of evaluation is as follows: for each of the experiments, all three of the scores are calculated between clustering  $C$  and  $\hat{C}$ . Computing the score each round rewards clustering algorithms that can detect the correct structure at an early stage of learning. On the other hand, it penalises methods that either perform clustering too early (resulting in the detection of an improper structure) or overcluster the population structure. Aggregated results for all four datasets across every possible split are plotted in Table 1. The clustering round is presented in the Table 2.

### 4.4 Local and Global Performance

The local and global performance visualises the trade-off between personalisation (the model’s ability to perform well on local learning tasks) and generalisation (the same ability but in relation to a broader set of examples, possibly performed in relation to out-of-cluster distribution). During this experiment, we define personalisation capabilities as the mean F1-score (PF1) averaged over all the client and training rounds. As noted before, the averaging values over all the iterations reward algorithms that can achieve better personalisation results at an early stage and penalise those that tend to run into sub-optimal solutions due to the incorrect clustering of clients. Moreover, it allows us to present results in one figure containing all the performed experiments. Generalisation, on the other hand, is defined as the mean F1-score (GF1) achieved on the uniformly distributed test set of the orchestrator. To visualise the trade-off between personalisation and generalisation, we define a metric called Learning Gap (LG) as follows:

**Definition 8 (Learning Gap (LG))** *Let  $h_{a_1}$  denote the hypothesis function obtained by following the training procedure  $a_1$ . Moreover, let  $D_{p_i}$  denote the dataset of a certain client  $i$  from population  $P$ , and let  $D_o$  denote the dataset of the orchestrator. Then, the LG is defined as follows:*

$$LG(h_{a_1}, D_{p_i}, D_o) = |f(h_{a_1}, D_{p_i}) - f(h_{a_1}, D_o)| \quad (11)$$

In practice, the chosen metric (e.g. Accuracy or F1Score) is substituted in place of a loss function in Definition 8 to obtain an easily comparable metric. Moreover, in a



		Non Overlapping						Overlapping					
		Balanced			Imbalanced			Balanced			Imbalanced		
		RAND	AMI	COM	RAND	AMI	COM	RAND	AMI	COM	RAND	AMI	COM
MNIST 15	SCL	0.44	0.46	0.57	0.57	0.57	0.57	0.21	0.31	0.57	0.29	0.38	0.57
	BCL	—	—	—	—	—	—	—	—	—	—	—	—
	OCFL-KM	<b>0.96</b>	<b>0.96</b>	<b>0.96</b>	<b>0.96</b>	<b>0.96</b>	<b>0.96</b>	<b>0.96</b>	<b>0.96</b>	<b>0.96</b>	<b>0.96</b>	<b>0.96</b>	<b>0.96</b>
	OCFL-AFF	0.23	0.27	0.26	0.13	0.06	0.12	0.23	0.27	0.26	0.30	0.30	0.30
	OCFL-MS	0.71	0.67	<b>0.96</b>	<b>0.96</b>	<b>0.96</b>	<b>0.96</b>	0.87	0.87	<b>0.96</b>	<b>0.96</b>	<b>0.96</b>	<b>0.96</b>
	OCFL-HDB	<b>0.96</b>	<b>0.96</b>	<b>0.96</b>	<b>0.96</b>	<b>0.96</b>	<b>0.96</b>	<b>0.96</b>	<b>0.96</b>	<b>0.96</b>	<b>0.96</b>	<b>0.96</b>	<b>0.96</b>
MNIST 30	SCL	0.45	0.49	0.57	0.57	0.58	0.57	0.19	0.30	0.57	0.26	0.33	0.57
	BCL	—	—	—	-0.04	-0.07	0.03	—	—	—	—	—	—
	OCFL-KM	<b>0.96</b>	<b>0.96</b>	<b>0.96</b>	0.96	0.96	0.96	0.90	0.90	0.90	<b>0.94</b>	<b>0.94</b>	<b>0.94</b>
	OCFL-AFF	0.38	0.44	0.37	0.66	0.63	0.65	0.36	0.42	0.35	0.50	0.49	0.42
	OCFL-MS	0.85	0.84	0.94	0.94	0.94	0.94	0.87	0.87	0.92	<b>0.94</b>	<b>0.94</b>	<b>0.94</b>
	OCFL-HDB	0.92	0.92	0.92	<b>0.98</b>	<b>0.98</b>	<b>0.98</b>	<b>0.94</b>	<b>0.94</b>	<b>0.94</b>	<b>0.94</b>	<b>0.94</b>	<b>0.94</b>
FMNIST 15	SCL	0.46	0.48	0.57	0.55	0.53	0.57	0.19	0.28	0.57	0.17	0.27	0.57
	BCL	-0.14	-0.23	0.00	—	—	—	—	—	—	—	—	—
	OCFL-KM	<b>0.98</b>	<b>0.98</b>	<b>0.98</b>	<b>0.98</b>	<b>0.98</b>	<b>0.98</b>	<b>0.98</b>	<b>0.98</b>	<b>0.98</b>	<b>0.98</b>	<b>0.98</b>	<b>0.98</b>
	OCFL-AFF	0.23	0.27	0.27	0.22	0.25	0.26	0.23	0.27	0.26	0.30	0.31	0.31
	OCFL-MS	<b>0.98</b>	<b>0.98</b>	<b>0.98</b>	<b>0.98</b>	<b>0.98</b>	<b>0.98</b>	<b>0.98</b>	<b>0.98</b>	<b>0.98</b>	<b>0.98</b>	<b>0.98</b>	<b>0.98</b>
	OCFL-HDB	0.96	0.96	0.96	<b>0.98</b>	<b>0.98</b>	<b>0.98</b>	0.96	0.96	0.96	<b>0.98</b>	<b>0.98</b>	<b>0.98</b>
FMNIST 30	SCL	0.57	0.57	0.57	0.57	0.58	0.57	0.42	0.43	0.57	0.53	0.52	0.57
	BCL	—	—	—	—	—	—	-0.07	-0.15	0.00	-0.05	-0.09	0.00
	OCFL-KM	0.96	0.96	0.96	<b>0.98</b>	<b>0.98</b>	<b>0.98</b>	<b>0.96</b>	<b>0.96</b>	<b>0.96</b>	0.96	0.96	0.96
	OCFL-AFF	0.39	0.45	0.37	0.66	0.64	0.67	0.37	0.43	0.36	0.51	0.50	0.43
	OCFL-MS	0.85	0.84	<b>0.98</b>	0.96	0.96	0.96	0.94	0.94	0.94	<b>0.98</b>	<b>0.98</b>	<b>0.98</b>
	OCFL-HDB	<b>0.98</b>	<b>0.98</b>	<b>0.98</b>	<b>0.98</b>	<b>0.98</b>	<b>0.98</b>	0.94	0.94	0.94	0.96	0.96	0.96
CIFAR 15	SCL	—	—	—	—	—	—	—	—	—	—	—	—
	BCL	0.00	0.00	0.60	0.00	0.00	0.60	0.00	0.00	0.60	0.00	0.00	0.60
	OCFL-KM	0.35	0.40	0.43	0.52	0.60	0.60	0.90	0.90	0.90	0.68	0.67	0.66
	OCFL-AFF	—	—	—	—	—	—	0.08	0.11	0.21	0.35	0.32	0.31
	OCFL-MS	0.23	0.26	0.57	0.16	0.18	0.58	—	—	—	0.73	0.67	0.73
	OCFL-HDB	<b>0.73</b>	<b>0.73</b>	<b>0.77</b>	<b>0.84</b>	<b>0.84</b>	<b>0.84</b>	<b>0.59</b>	<b>0.59</b>	<b>0.69</b>	<b>0.77</b>	<b>0.77</b>	<b>0.74</b>
CIFAR 30	SCL	—	—	—	—	—	—	—	—	—	—	—	—
	BCL	0.00	0.00	0.60	0.00	0.00	0.60	0.00	0.00	0.60	0.00	0.00	0.60
	OCFL-KM	0.37	0.54	0.51	0.42	0.56	0.56	<b>0.90</b>	<b>0.90</b>	<b>0.90</b>	0.59	0.55	0.58
	OCFL-AFF	0.35	0.41	0.34	0.46	0.45	0.39	0.23	0.22	0.20	0.32	0.30	0.26
	OCFL-MS	0.63	0.55	0.86	0.56	0.63	0.58	—	—	—	—	—	—
	OCFL-HDB	<b>0.77</b>	<b>0.77</b>	<b>0.77</b>	<b>0.88</b>	<b>0.88</b>	<b>0.88</b>	0.64	0.64	0.69	<b>0.83</b>	<b>0.83</b>	<b>0.81</b>
PATHMNIST 15	SCL	—	—	—	—	—	—	—	—	—	—	—	—
	BCL	0.00	0.00	0.60	0.00	0.00	0.60	0.00	0.00	0.60	0.00	0.00	0.60
	OCFL-KM	<b>0.96</b>	<b>0.96</b>	<b>0.96</b>	<b>0.96</b>	<b>0.96</b>	<b>0.96</b>	0.50	0.62	0.60	0.96	0.96	0.96
	OCFL-AFF	0.23	0.27	0.27	0.12	0.13	0.16	0.08	0.06	0.12	0.22	0.25	0.26
	OCFL-MS	0.78	0.80	0.98	0.38	0.58	0.46	0.45	0.55	0.62	<b>0.96</b>	<b>0.96</b>	<b>0.96</b>
	OCFL-HDB	0.94	0.94	0.94	<b>0.96</b>	<b>0.96</b>	<b>0.96</b>	<b>0.88</b>	<b>0.88</b>	<b>0.98</b>	<b>0.96</b>	<b>0.96</b>	<b>0.96</b>
PATHMNIST 30	SCL	—	—	—	—	—	—	—	—	—	—	—	—
	BCL	0.00	0.00	0.60	0.00	0.00	0.60	0.00	0.00	0.60	0.00	0.00	0.60
	OCFL-KM	<b>0.98</b>	<b>0.98</b>	<b>0.98</b>	<b>0.96</b>	<b>0.96</b>	<b>0.96</b>	0.51	0.58	0.60	0.98	0.98	0.98
	OCFL-AFF	0.39	0.45	0.37	0.29	0.36	0.29	0.39	0.45	0.37	0.32	0.30	0.35
	OCFL-MS	0.45	0.60	0.57	0.45	0.64	0.49	0.51	0.60	0.63	<b>0.98</b>	<b>0.98</b>	<b>0.98</b>
	OCFL-HDB	<b>0.98</b>	<b>0.98</b>	<b>0.98</b>	<b>0.96</b>	<b>0.96</b>	<b>0.96</b>	<b>0.54</b>	<b>0.54</b>	<b>0.57</b>	<b>0.98</b>	<b>0.98</b>	<b>0.98</b>
BLOODMNIST 15	SCL	—	—	—	—	—	—	—	—	—	—	—	—
	BCL	0.00	0.00	0.60	0.00	0.00	0.60	0.00	0.00	0.60	0.00	0.00	0.60
	OCFL-KM	<b>0.98</b>	<b>0.98</b>	<b>0.98</b>	<b>0.92</b>	<b>0.92</b>	<b>0.92</b>	<b>0.98</b>	<b>0.98</b>	<b>0.98</b>	<b>0.98</b>	<b>0.98</b>	<b>0.98</b>
	OCFL-AFF	0.23	0.27	0.27	0.12	0.13	0.16	0.23	0.27	0.27	0.31	0.31	0.31
	OCFL-MS	0.78	0.80	<b>0.98</b>	<b>0.92</b>	<b>0.92</b>	<b>0.92</b>	0.83	0.86	0.98	0.65	0.74	<b>0.98</b>
	OCFL-HDB	<b>0.98</b>	<b>0.98</b>	<b>0.98</b>	<b>0.92</b>	<b>0.92</b>	<b>0.92</b>	<b>0.98</b>	<b>0.98</b>	<b>0.98</b>	<b>0.98</b>	<b>0.98</b>	<b>0.98</b>
BLOODMNIST 30	SCL	—	—	—	—	—	—	—	—	—	—	—	—
	BCL	0.00	0.00	0.60	0.00	0.00	0.60	0.00	0.00	0.60	0.00	0.00	0.60
	OCFL-KM	<b>0.98</b>	<b>0.98</b>	<b>0.98</b>	<b>0.98</b>	<b>0.98</b>	<b>0.98</b>	<b>0.98</b>	<b>0.98</b>	<b>0.98</b>	<b>0.54</b>	<b>0.62</b>	<b>0.66</b>
	OCFL-AFF	0.39	0.45	0.37	0.50	0.50	0.43	0.39	0.45	0.37	0.32	0.37	0.32
	OCFL-MS	0.93	0.93	<b>0.98</b>	<b>0.98</b>	<b>0.98</b>	<b>0.98</b>	0.53	0.67	0.59	<b>0.54</b>	<b>0.62</b>	<b>0.66</b>
	OCFL-HDB	<b>0.98</b>	<b>0.98</b>	<b>0.98</b>	<b>0.98</b>	<b>0.98</b>	<b>0.98</b>	<b>0.54</b>	<b>0.54</b>	<b>0.57</b>	0.48	0.48	0.48

Table 1: Clustering performance measured in terms of Rand Index (RAND), Adjusted Mutual Information Score (AMI) and Completeness Score (COM) for all datasets (with a number of clients equal to 15 or 30), data splits, and across six different clustering algorithms: Sattler et al. (2021) (SCL), Briggs et al. (2020) (BCL), OCFL with K-Means Algorithm (OCFL-KM), OCFL with Affinity Algorithm (OCFL-AFF), OCFL with Mean-Shift algorithm (OCFL-MS) and OCFL with HDBSCAN algorithm (OCFL-HDBS). The double hyphen (—) is placed if the algorithm has failed to perform any clustering in the given scenario.

Dataset	Algorithm	Non Overlapping		Overlapping	
		Balanced	Imbalanced	Balanced	Imbalanced
MNIST 15	SCL	31	23	25	24
	BCL	21	21	21	21
	OCFL-KM	3	3	3	3
	OCFL-AFF	3	3	3	4
	OCFL-MS	3	3	3	3
	OCFL-HDB	3	3	3	3
MNIST 30	SCL	44	23	35	34
	BCL	21	21	21	21
	OCFL-KM	3	3	6	4
	OCFL-AFF	3	4	5	4
	OCFL-MS	4	4	5	4
	OCFL-HDB	5	2	4	4
FMNIST 15	SCL	46	24	34	35
	BCL	21	21	21	21
	OCFL-KM	2	2	2	2
	OCFL-AFF	2	3	3	3
	OCFL-MS	2	2	2	2
	OCFL-HDB	3	2	3	2
FMNIST 30	SCL	23	23	50	50
	BCL	21	21	21	21
	OCFL-KM	3	2	3	3
	OCFL-AFF	2	3	4	3
	OCFL-MS	2	3	4	2
	OCFL-HDB	2	2	4	3
CIFAR10 15	SCL	–	–	–	–
	BCL	21	21	21	21
	OCFL-KM	8	6	6	6
	OCFL-AFF	6	6	6	7
	OCFL-MS	5	7	6	7
	OCFL-HDB	5	9	5	6
CIFAR10 30	SCL	–	–	–	–
	BCL	21	21	21	21
	OCFL-KM	7	8	6	7
	OCFL-AFF	7	8	6	7
	OCFL-MS	8	7	6	7
	OCFL-HDB	8	7	7	6
PATHMNIST 15	SCL	–	–	–	–
	BCL	21	21	21	21
	OCFL-KM	3	3	3	3
	OCFL-AFF	2	4	2	3
	OCFL-MS	2	3	4	3
	OCFL-HDB	4	3	2	3
PATHMNIST 30	SCL	–	–	–	–
	BCL	21	21	21	21
	OCFL-KM	2	3	2	2
	OCFL-AFF	2	4	2	2
	OCFL-MS	2	3	2	2
	OCFL-HDB	2	3	2	2
BLOODMNIST 15	SCL	–	–	–	–
	BCL	21	21	21	21
	OCFL-KM	2	5	2	2
	OCFL-AFF	2	5	2	2
	OCFL-MS	2	5	2	2
	OCFL-HDB	2	5	2	2
BLOODMNIST 30	SCL	–	–	–	–
	BCL	21	21	21	21
	OCFL-KM	2	2	2	2
	OCFL-AFF	2	2	2	2
	OCFL-MS	2	2	2	2
	OCFL-HDB	2	2	2	2

Table 2: Table presenting the clustering round for all datasets (with a number of clients equal to 15 or 30), data splits, and across six different clustering algorithms: Sattler et al. (2021) (SCL), Briggs et al. (2020) (BCL), OCFL with K-Means Algorithm (OCFL-KM), OCFL with Affinity Algorithm (OCFL-AFF), OCFL with MeanShift algorithm (OCFL-MS) and OCFL with HDBSCAN algorithm (OCFL-HDBS). The double hyphen (–) is placed if the algorithm has failed to perform any clustering in the given scenario. In the case of the Sattler et al. (2021) algorithm, the last clustering round is displayed.

controlled experimental setting, we opted for a uniformly distributed dataset across the labels for an orchestrator test set  $D_o$ . We utilise the fact that, as described in the Section 4.1, the orchestrator dataset consists of a held-out test dataset, which makes it a proper candidate for testing the generalisation capabilities of the model. Ideally, the model should be characterised by a high F1-score achieved on a local dataset and a small learning gap. It would imply that the model has achieved high personalisation capabilities while retaining a high degree of general knowledge. On the other hand, a low PF1 with a low DIST score would imply that the model has not been personalised. The results of the experiments are presented in Figure 2.

#### 4.5 Behaviour of Temperature Function

In order to evaluate the behaviour of the Temperature Function (Definition 7) that is used as a method of detecting suitable clustering moment, we register the temperature of the baseline cluster each round for all the experiments performed on the five selected datasets. Visualisation of the experiments is reported in Figure 3. Each plot presents a stacked representation of each task in a given number of clients. A solid blue line symbolises the mean across all the scenarios (overlapping and non-overlapping in balanced and imbalanced settings). Blue shadow represents confidence intervals established based on the variations between different scenarios. The temperature function is normalised in  $[0, 1]$  for comparison purposes. As explained in the Section 3.2, this can be done easily with a scaling constant  $\lambda$ . However, it does not have any practical effect on the efficiency of Algorithm 1 and was done in order to render the visualisation more accessible.

Moreover, Figure 4 presents an averaged behaviour of the Temperature Function across all the datasets with corresponding confidence intervals. This graph should be approached with caution, as the data presented on it combines tasks from the same domain (classification in computer vision) but performed on different datasets. However, since it can also be interpreted as *on-average* behaviour of the Temperature Function, it is presented together with individual averages displayed in Figure 3. Individual graphs for each particular run are placed in the appendix to this paper under the Subsection A.3.

#### 4.6 Discussion

##### 4.6.1 PERFORMANCE

An overview of the experimental data can indicate the high performance of the OCFL algorithm, especially when it is combined with density-based methods such as Meanshift or HDBSCAN. In terms of clustering performance (section 4.3), OCFL-HDB and OCFL-MS often outperform all other compared algorithms, with the RAND scores around 0.95 on all splits across the MNIST dataset, 0.96 across the FMNIST dataset and 0.80 across the CIFAR10 dataset (Table 1). Similar values (ranging from 0.80 to 0.98) hold on the PathMNIST and BloodMNIST datasets. From all the presented splits, Overlapping Balanced seems to be the most challenging, as even the OCFL-HDB and OCFL-MS exhibit sometimes lower RAND values on that particular split (around 0.60 for OCFL-HDB on CIFAR 15 and CIFAR 30 and around 0.5 for OCFL-MS for PathMNIST 15 and PathMNIST 30), while sometimes even failing altogether to distinguish more than one cluster (the case of

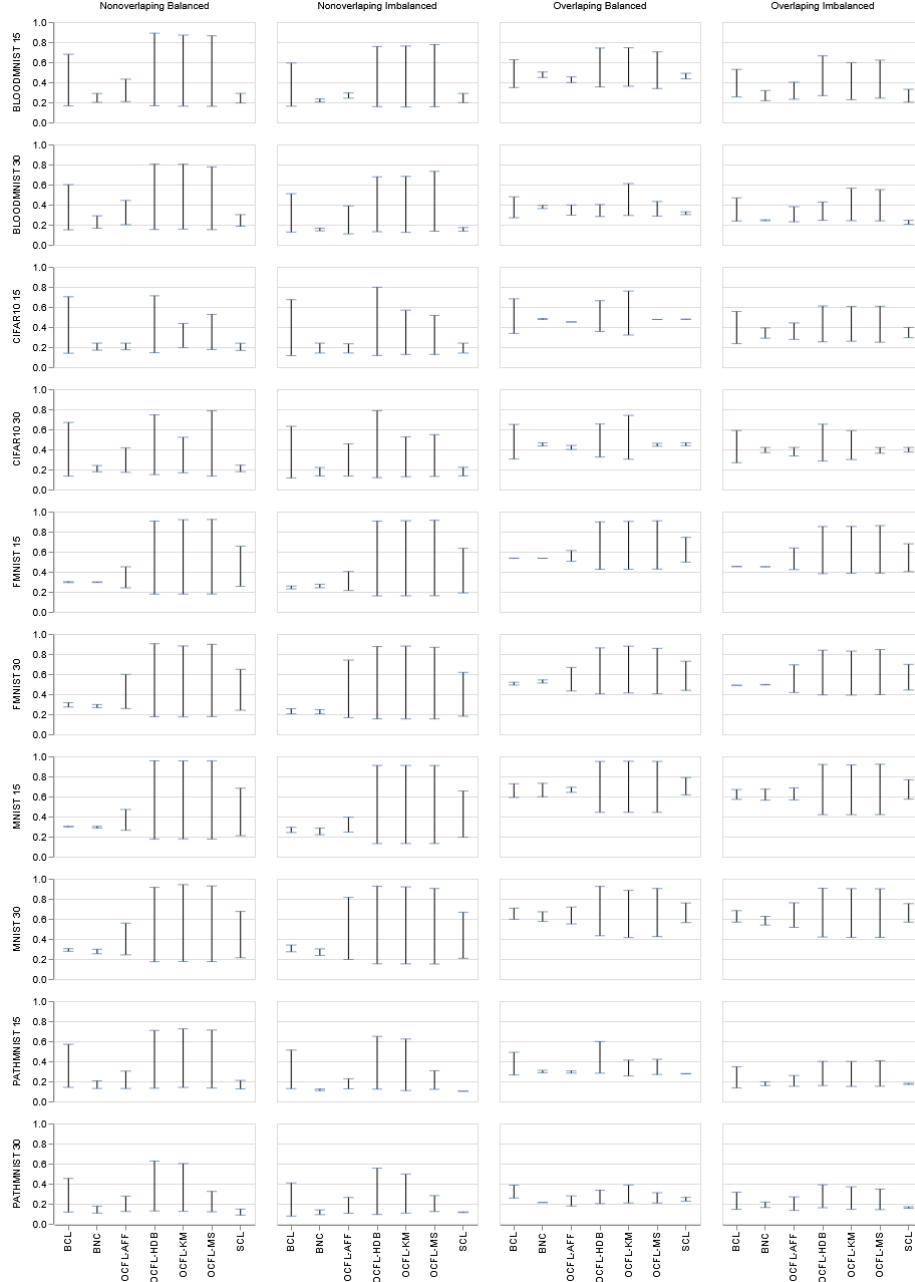


Figure 2: Average performance of models in terms of F1-score. In the plot, the lower part of each segment indicates generalised F1-score (GF1), while the upper part indicates personalised F1-score (PF1). The length of the segment represents the learning gap as defined in Equation 8. The GF1 is calculated using a hold-out test set that is uniformly distributed across all the classes. The PF1 is calculated using a local test set - a hold-out sample taken from the local training set before the start of the training for each of the nodes.

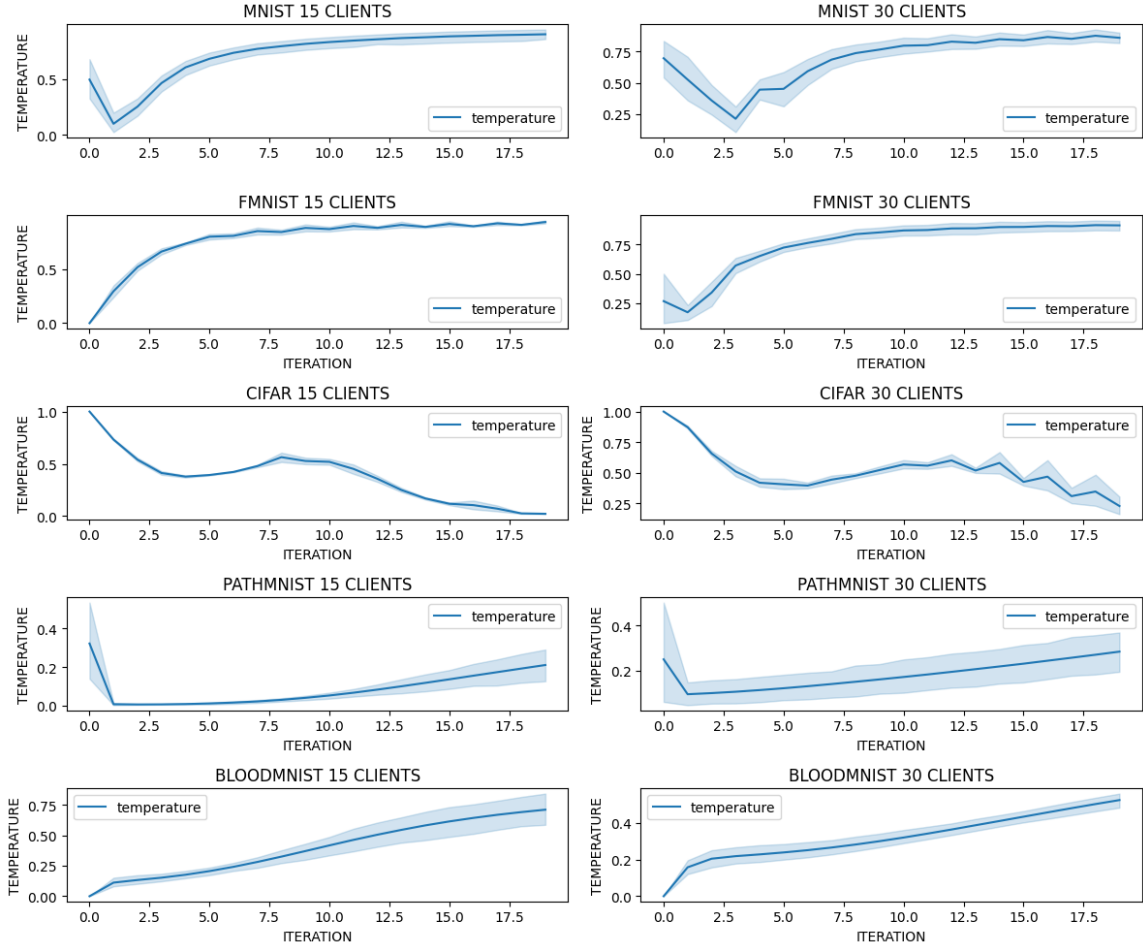


Figure 3: Behaviour of the (normalised) Temperature Function as defined in the Definition 7. A solid blue line symbolises the mean across all the scenarios (overlapping and non-overlapping with balanced and imbalanced settings). Blue shadow represents confidence intervals established based on the variations between different scenarios.

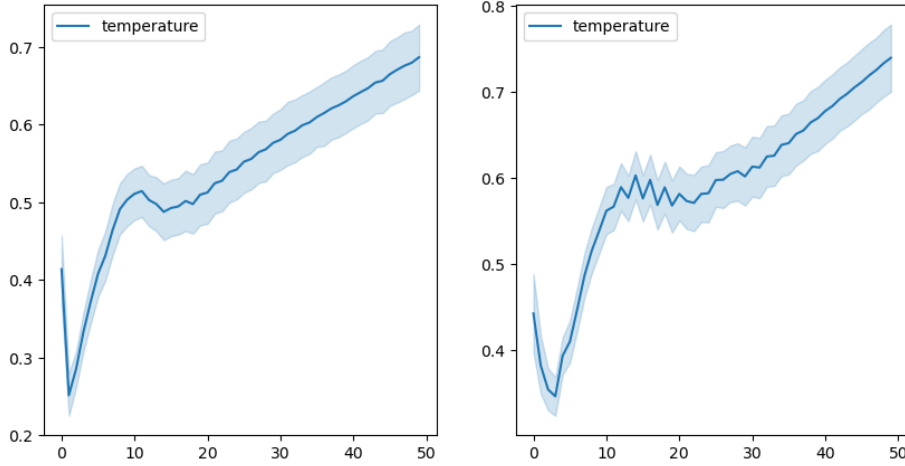


Figure 4: Behaviour of the (normalised) Temperature Function as defined in the Definition 7 averaged across all the data runs and data splits. A solid blue line symbolises the mean across all the scenarios (overlapping and non-overlapping with balanced and imbalanced settings). Blue shadow represents confidence intervals established based on the variations between different scenarios and datasets. The average for 15 clients is placed on the left, while the average for 30 clients is placed on the right.

OCFL-MS on CIFAR 15 and CIFAR 30). This is not surprising given the close resemblance of local distributions under those circumstances.

Regarding all the other cases, such a high RAND and Adjusted Mutual Information Score imply that both algorithms are able to almost perfectly distinguish between clusters at a very early stage, correctly separating cohorts of clients. Another key observation drawn from the data is the general difficulty of the distance-based algorithms, and it concerns State-of-the-Art algorithms (such as those introduced by Briggs et al. (2020) and Sattler et al. (2021)) and OCFL-AFF alike. Usage of those algorithms requires a proper hyper-tuning of hyperparameters, which is especially challenging in the federated environment. Although we followed the general guidelines presented in both articles and performed a reduced grid search, reporting only the highest recorded values, the failure to cluster the clients into more than one or two clusters clearly indicates that those methods may often work well as a post-processing method. However, their use as a pre-processing (or in-training) clustering method may be problematic due to limited knowledge about the proper set of hyperparameters.<sup>7</sup> There is also a clear correlation between SCL (Sattler et al. (2021)), BCL (Briggs et al. (2020)) and OCFL-AFF. In cases where the limited grid search has returned a viable solution, those three algorithms tend to behave relatively well. However, when the grid search was initialised beyond the probable optimal region of search, the algorithms tended to run into multiple issues, with the total lack of clustering as the most severe one. It must be noted that a second additional hypertuning method was employed in

7. Indeed, there is a clear indication in both works of Sattler et al. (2021) and Briggs et al. (2020) (which we do not assess in this work) that the presented methods are a perfect solution for post-processing performed in the Federated setting.

the case of Sattler et al. (2021), which was described in detail in Subsection 4.2 and which relied on the measurements of gradients in the pre-trained centralised version of the model. However, this method also failed in many cases, returning a one cluster.

The proper clustering should be reflected in the performance of personalised models, and this is the case as presented in Subsection 4.4. The baseline model is characterised by an F1-score between the range of 0.24 (CIFAR10 dataset as illustrated in 2) and 0.6 (for MNIST dataset). However, the local models delivered by the OCFL-MS and OCFL-HDB achieve an F1-score between 0.96 (MNIST) and 0.65 (CIFAR10). Based on that figure, we could distinguish a **performance upper bound** that measures the ability of the model to solve the task locally and **performance lower bound** that measures the ability of the model to solve the task on a broader set of examples, possible out-of-distribution. What must be noted is the relatively high performance upper bound for all the OCFL algorithms. It means that they can deliver an accurate and higher than compared State-of-the-Art solution for personalisation of local learning. On the other hand, the family of OCFL algorithms generally tend to have similar or only slightly lower *performance lower bound*, which would imply that the loss of generalisation capabilities is not detrimental when compared to other clustering methods. Figure 2 can illustrate it quite well, as the generalised F1-score (lower part of each segment) is more or less comparable for all the presented methods, with the baseline serving as the most generalised case for obvious reasons. However, the personalised F1-score (higher part of each segment) is visibly better for the family of OCFL methods, with particular emphasis on the high effectiveness of the OCFL-HDB. In future research directions, we address the issue of lowering the Learning Gap as defined in Definition 8, potentially transferring knowledge between different clusters.

It must also be highlighted that all four data splits generated for the experiments were challenging. Contrary to the label swaps or other similar methods often employed in studies of CFL, the presented data splits assume more subtle differences in the data distribution as described in Subsection 4.1. Such a subtlety may confound many clustering algorithms. Hence, a weaker performance of the OCFL-Kmeans or OCFL-Affinity, in line with the failures of algorithms presented in Briggs et al. (2020) and Sattler et al. (2021) to distinguish nodes and attribute them to more than one cluster. In this context, a high performance of density-based algorithms is an even more valuable insight.

A final note should be made regarding an assumption that, due to the high-dimensionality of the feature space, the clustering will yield a less than optimal solution (such a statement is provided by, inter alia, Ghosh et al. (2022)). As explained in the introductory part of this paper, we tried to avoid clustering in lower-dimensional spaces using embedding and dimensionality reduction techniques such as those presented by Duan et al. (2021). The reason for that is twofold. Firstly, as explained, we are interested in a clustering-agnostic solution that is suitable for a variety of different clustering algorithms, and dimensionality reduction could possibly negatively impact some of the tested algorithms. Secondly, dimensionality reduction would inevitably result in information loss; hence, a strong empirical proof of its necessity would be required. However, as evidenced by our empirical tests, the performance of K-Means, Mean Shift and HDBSCAN stays comparatively high while still employing the full set of provided gradients. This is an additional observation that was made during our studies, one that put into question the commonly encountered narrative that simply

calculating cosine distance (or cosine similarity) on the pseudo-loss surface reconstructed from the federated gradients is ineffective due to the high dimensionality of the latter.

#### 4.6.2 BEHAVIOUR OF THE TEMPERATURE FUNCTION

A different part of the discussion should be dedicated solely to the behaviour of the Temperature Function as defined in Definition 7. One can distinguish two separate aspects that should be discussed: **(i)** behaviour of the Temperature Function at the beginning of the training and **(ii)** asymptotic behaviour of that function that can be observed.

Concerning the first part of the previous statement, it can be concluded that preliminary assumptions made in Subsection 3.3 generally empirically hold. That means, that two possible outcomes may be observed: **(i)** either the similarity of the local networks trained on incongruent data distributions will increase (hence, the chosen distance measure and, in turn, the Temperature Function will decrease) before reaching a local minimum and then diverging due to said incongruence or **(ii)** the similarity of the local networks will drop steadily from the very first round, never reaching a local minimum. The first case was predominantly observed on the MNIST and CIFAR10 datasets, while the second case was predominantly observed on the FMNIST and PATHMNIST datasets. The BloodMNIST dataset falls in either of those categories, depending on the evaluated data split. In both cases, the OCFL will succeed in clustering, either clustering after a local minimum or at the second round of the global training.

Concerning the asymptotic behaviour of the Temperature Function, two different cases were observed. Either **(i)** the similarities of the local gradients are rising consistently after a certain number of rounds (each local model *pulls* into its own direction) or **(ii)** a total network collapse happens after which the gradients become uninformative. The first case is much more predominant in the conducted experiments, ranging from MNIST, FMNIST, to PATHMNIST and BLOODMNIST datasets on all four splits, either in a 15 or 30-client scenario. The second case is limited only to CIFAR-10. Initially, we assumed that the Temperature Function dropping to 0 on that dataset may imply that the baseline FedAvg or FedOpt algorithms are able to converge while solving this task, "reconciling" together incongruent data distributions. However, this is not backed up by any empirical evidence, especially the relatively poor generalisability of the baseline model on this task (Figure 2). Moreover, we theorised that the Temperature Function dropping to 0 fundamentally implies that the local models (after performing 3 local epochs) are the same, even though their local distribution is vastly different. The only other convincing hypothesis regarding this behaviour concerns model collapse - that the incongruence of the local distribution ultimately causes the gradients to be uninformative, locking them in a region from which the local models can no longer escape through backpropagation. What must be additionally noted is that the asymptotic behaviour of the Temperature Function does not concern the OCFL algorithm to the same degree as the initial behaviour does. Even assuming that the CIFAR10 model indeed converges, then there is still a clear advantage of performing clustering, as evidenced by the performance gain displayed in Figure 2.



## 5 Cluster-Level Explainability

This Section contains an additional part of the experiments conducted on OCFL algorithm, as well as on the effects of the personalisation on explainability in general. The preliminary (intuitive) assumption would be that the personalised model should be able to deliver more precise and cohesive explanations on the local dataset than one that is not personalised. The experimental setup is discussed in Subsection 5.1. The visual inspection of individual explanations is done in Subsection 5.2, and the formal quantitative assessments are overviewed in Subsections 5.3 and 5.2.

### 5.1 Experimental Setup

The evaluation of explanations’ quality based on saliency maps is a challenging and unresolved problem. As noted by Kindermans et al. (2019), there does not exist a well-defined metric that would allow for a direct quantitative comparison of the generated maps. Nevertheless, based on the methods introduced by Petsiuk et al. (2018), we design an evaluation framework that allows us to compare the characteristics of saliency maps. The authors of Petsiuk et al. (2018), based partially on the work of Fong and Vedaldi (2017), introduced two autonomous metrics for evaluating the quality of the generated heat maps: *insertion* and *deletion* metrics. The intuition behind those two metrics is connected to the assumption that a ”good” explanation should always target only the most important pixels in the image. Hence, given an image and a label, if deletion of just a few most important pixels<sup>8</sup> will cause a rapid drop of classifier certainty, it will imply that the explanation method has correctly identified the most important part of the image. On the contrary, if the insertion of just a few crucial pixels will give a sudden rise to a classifier’s certainty, it would similarly imply that the heatmap has correctly identified crucial parts of the feature space, upon which an attribution to a particular class depends. The process of adding and removing pixels can be divided into  $\lceil \frac{W \times H}{s} \rceil$ , where  $W$  and  $H$  are the width and the height of the image and  $s$  is a step-size controlling how many pixels are we adding (or removing) at once. Additionally, upon each step, the probability of a target class is calculated, allowing one to calculate the total area under the curve (AUC) for each image. For the deletion metric, a low AUC would imply a sharp decrease in classifier confidence upon removing just a few most critical pixels, as indicated by the saliency map, and thus would imply a ”good” quality of the classifier. The high AUC would indicate the same for the insertion metric.

One of the key challenges of adapting this method to the presented scenario was the fact that we are not interested as much in the difference between particular explainers as the general tendency of the explanation across different clusters across different scenarios and algorithms. Hence, we had to design an evaluation framework that would provide aggregated statistics of explanation quality across different experimental runs for different algorithms - something that the original method was not suited for.

In order to do that, an experimental framework was designed. For each possible simulation run, we concatenate the individual insertion and deletion scores calculated for specific

---

8. Where the importance is based on the local values of the saliency map.

clusters.<sup>9</sup> Afterwards, we calculate measurements such as mean, variance or quartile values representing the distribution of explanations generated by a hypothesis function belonging to a particular cluster. This allows us to summarise an individual simulation run irrespective of how many clusters the population of clients was actually divided into. The rationale of such a framework is connected to the fact that if the population was divided into clusters that are characterized by hypothesis functions that are easy to interpret, the average AUC of insertion metric (calculated across all the clusters) would be high.<sup>10</sup> However, even one bad cluster of clients that is characterised by an unexplainable hypothesis function can ruin the assessment, resulting in a worse score for the whole algorithm in the given setting. This also allows us to easily compare the average value of insertion and deletion metrics across the different simulation runs and, hence, compare the quality of explanations for different clustering algorithms.

The precise methodology of the assessment is presented in Algorithm 2. The first step is to define it as an assessed scenario (e.g. HDBSCAN clustering for 15 clients holding the MNIST dataset in an overlapping and imbalanced split). Subsequently, one fixes an iteration from which the models will be assessed (conventionally, it is the last iteration of the training or at least the last iteration of the training from which the models were preserved). For each client, it is possible to generate *in-sample*, *out-of-sample* and *orchestrator* distributions. The in-sample distribution consists of concatenated test sets of all the clients belonging to the same cluster. Out-of-sample distribution is formed by concatenating the test sets of all the clients not belonging to a certain cluster. Orchestrator distribution simply consists of data points sampled from an orchestrator test set. Afterwards, we sample a portion of the dataset formed in that way, feed the individual examples (or batches of examples as in this case) into the local model’s hypothesis function and generate explanations together with calculating insertion and deletion scores. Finally, we aggregate the results and calculate respective statistics for each of the clusters to either visualise that in the format of the box plots (where clusters represent particular data points) (Subsection 5.3 or perform Critical-Difference analysis (Subsection 5.4). The sample size (lines 3 and 14 of Algorithm 2) was chosen to be equal to 350 for MNIST, FMNIST, CIFAR10 and PathMNIST and 180 for BloodMNIST.

## 5.2 Qualitative Analysis of Saliency Maps

Visual inspection of the saliency maps generated by the local hypothesis functions on the dominant class (the class that the clustering should personalise towards) is the first step of the analysis. One of the undeniable advantages of the saliency-based explainability method (as presented by Samuel et al. (2021)) is the ability to plot and compare them easily against each other. This can serve as a preliminary check of the personalisation impact on the explainability.

For this experiment, we selected three clients for each dataset (clients 1, 7 and 12). The majority class is sampled from local test sets of each client, and an explanation is generated using hypothesis functions personalised by various clustering algorithms. Those results are

---

9. In fact, to speed up the process, our implementation envisages calculating the AUC scores across batches of the examples and then averaging the results before calculating the AUC score for that average, identically to the implementation presented by Petsiuk et al. (2018).  
 10. The same, although with a flipped value, would be true for the deletion metric.

**Algorithm 2:** Insertion-Deletion Framework for OCFL

---

```

1 input  $\mathcal{E}(\cdot)$ , Explainer
2 input  $T \in \mathbb{N}$ , Evaluation Round
3 input  $\zeta \in \mathbb{R}$   $\zeta \leq 1$ , Sample Size
4 input  $\mathbf{I} \in \{InDistribution, OutOfDistribution, Orchestrator\}$ , Evaluation Mode
5  $C_i^{INDE} \leftarrow \{\}$   $\forall C_i \in C$ 
6 for  $C_i \in C$  do
7    $\hat{h}_i = \frac{1}{|C_i|} \sum_{j \in C_j} \theta_j^{T,k}$ 
8   if  $\mathbf{I} == InDistribution$  then
9      $\hat{D} = \{D_k^{test} \in D | k \in C_j\}$ 
10  if  $\mathbf{I} == OutOfDistribution$  then
11     $\hat{D} = \{D_k^{test} \in D | k \notin C_j\}$ 
12  if  $\mathbf{I} == Orchestrator$  then
13     $\hat{D} = D_{orchestrator}$ 
14   $\hat{D} \leftarrow Sample(\hat{D}, \zeta)$ 
15   $e = AUC(\mathcal{E}(\hat{h}_i(x_i, y_i)))$ 
16   $C_i^{INDE} = C_i^{INDE} \cup e$ 
17 return  $C_1, C_2, \dots, C_n$ 

```

---

then plotted for each sampled data point individually. An example of such a comparison is displayed in Figure 5. Other visualisations are moved to the Appendix (Section A.4). The visualisations are only generated for the CIFAR10, PATHMNIST, and BLOODMNIST datasets. The reason for that is connected to the lower readability of the saliency maps when plotted together with greyscale images.

The qualitative analysis of the saliency maps delivers a few valuable observations. Firstly, the saliency maps generated by models personalised by OCFL-KM, OCFL-MS or OCFL-HDBS tend to generate fewer *artefacts* - unexplainable highlights that seem not to contain any substantial part of the image relevant for classification. They also tend to be more cohesive and focused on either the object itself or the direct surroundings of it, which may help the classifier to differentiate between the classes. The second observation concerns the relationship between the generated saliency map and a predicted class. There are examples of cases where the generated saliency maps were barely recognisable from each other, yet the predicted class was different. In that regard, OCFL-KM, OCFL-MS and OCFL-HDBS tend to predict the correct class more frequently. As pointed out earlier, the usability of qualitative analysis of individual saliency maps is rather limited in its nature (as explained by Kindermans et al. (2019), Petsiuk et al. (2018) and Samuel et al. (2021)), and this display is made predominantly for demonstration purposes only. The next two subsections deal with a more formal analysis of the generated explanations.

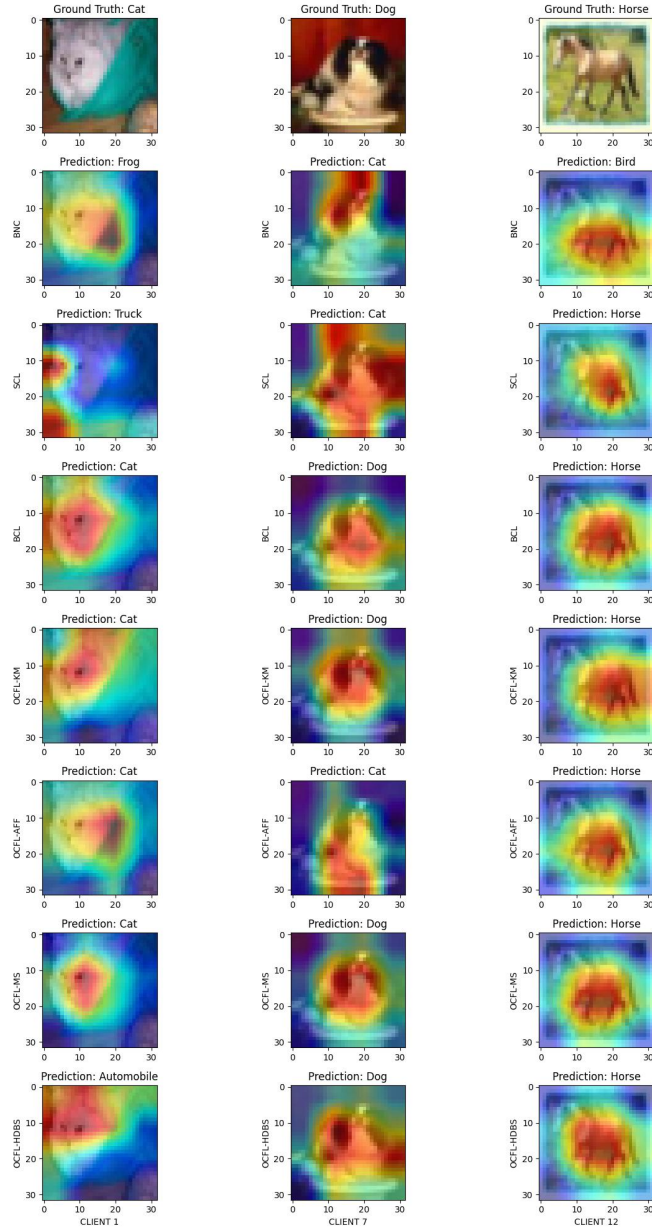


Figure 5: Showcase of the various saliency maps generated using seven different local models trained by various clustering algorithms on a CIFAR10 dataset: Baseline (BNC), Sattler et al. (2021) (SCL), Briggs et al. (2020) (BCL), OCFL with K-Means (OCFL-KM), OCFL with Affinity (OCFL-AFF), OCFL with MeanShift (OCFL-MS) and OCFL with HDBSCAN (OCFL-HDBS). Each column represents a different client, while each row represents a different clustering algorithm. Additionally, the true and predicted classes are placed above the images.

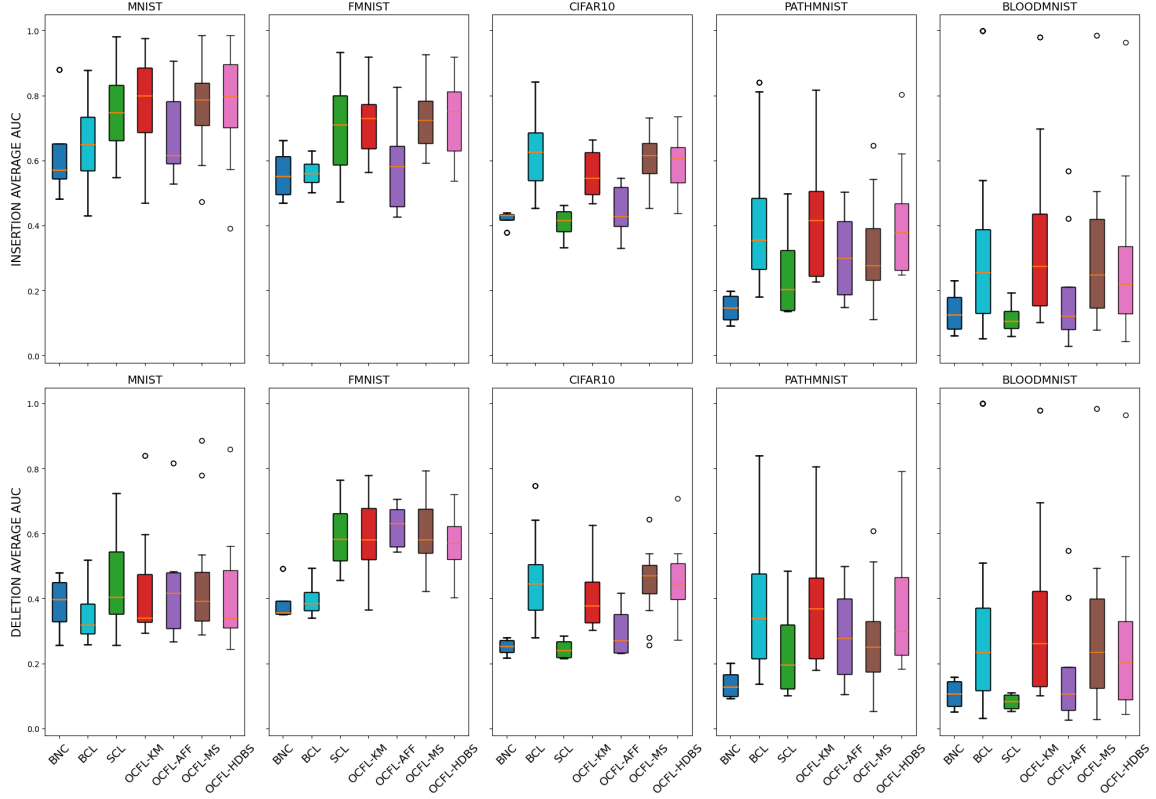


Figure 6: Boxplots for average insertion area under the curve (AUC) registered for particular clusters for **in-cluster distributions**. Each dataset is plotted as a separate column, and average inter-cluster insertion is placed in the first row, while average inter-cluster deletion is placed in the second row. One figure contains box plots of all six compared clustering algorithms and one additional plot for a baseline.

### 5.3 Inter Cluster Average AUC for Insertion and Deletion

The Algorithm 2 provides for calculating the average insertion and deletion scores for all clusters on either in-cluster, out-of-cluster or orchestrator distributions. Hence, for each particular dataset, data split, and algorithm, it is possible to obtain the average AUC for insertion-deletion and assess the variability of the AUC between the clusters. We perform those experiments in the following manner. Firstly, using algorithm 2, we calculate (in batches) the average AUC for insertion and deletion across the batch.<sup>11</sup> Afterwards, we average those scores, so that a single statistic represents each cluster. Given that we are interested in inter-cluster differences, we employ boxplots to assess the variability of those statistics across different splits within the area of one dataset. The final results are plotted in Figure 6 for samples sampled from the in-cluster distribution and in Figure 7 for data points samples from the orchestrator distribution.

11. The same method was used by Petsiuk et al. (2018) to calculate average AUC across the batches of data to speed up the process. This method was adopted directly from the repository of this paper available at the following link.

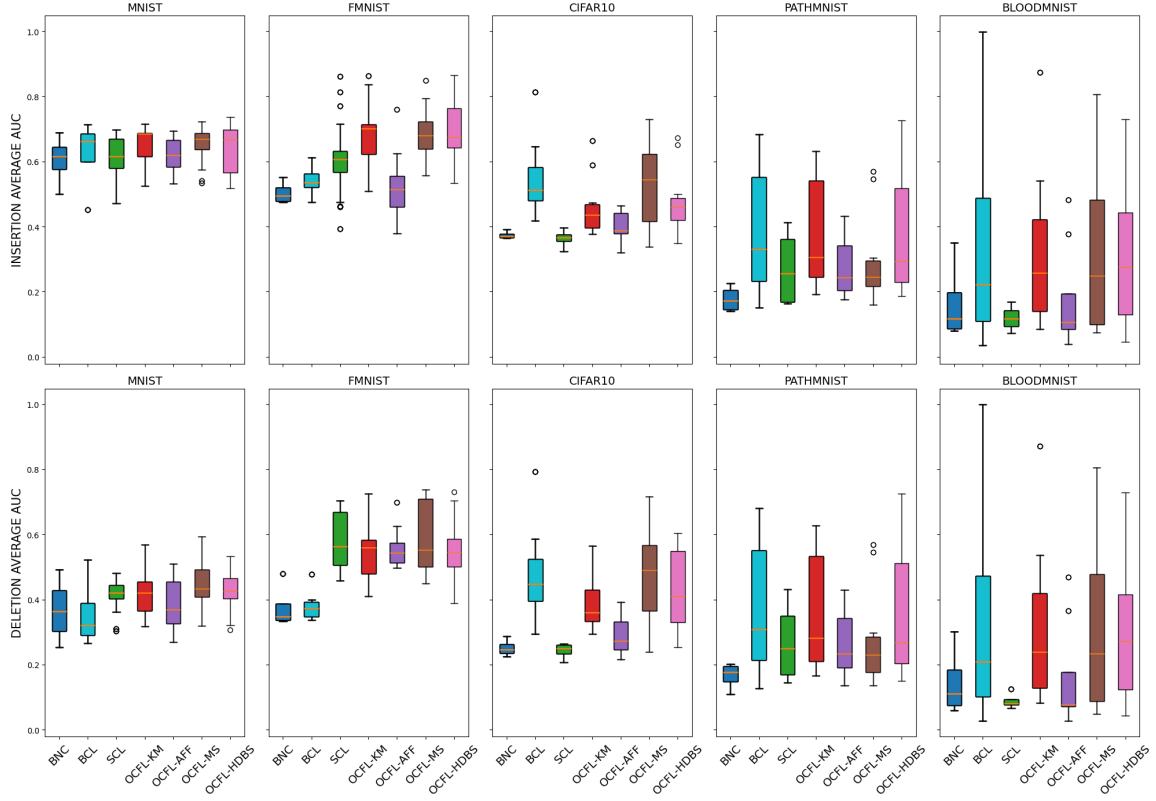


Figure 7: Boxplots for average insertion area under the curve (AUC) registered for particular clusters for **orchestrator distribution**. Each dataset is plotted as a separate column, and an average inter-cluster insertion is placed in the first row, while an average inter-cluster deletion is placed in the second row. One figure contains box plots of all six compared clustering algorithms and one additional plot for a baseline.

### 5.4 Critical Differences Analysis

Critical Differences analysis (CD) is a more rigorous approach to exploring the quantitative differences in the quality of explanations generated by a particular hypothesis function. The method of CD diagrams was first introduced by Demsar (2006) to compare outcomes of multiple different learning algorithms over multiple different datasets. The test is formally divided into two stages. Firstly, a Friedman test is performed to reject (or fail to reject) a hypothesis that there exist any significant differences in the tested methods. Then, a multiple hypothesis testing is performed (for example, with adjusted Wilcoxon test or with Bonferroni’s method) for each group of methods. Subsequently, the grouped methods are ranked and place on the x-axis. The groups that could not be statistically deemed as different are linked by a horizontal crossbar (as explained by Demsar (2006) or Mirko Bunse).

In the case of this study, the CD method allows one to compare the insertion and deletion scores of various algorithms over multiple (repeated) test runs. In order to do that, an average across all clusters is calculated.<sup>12</sup> The results for the *in-distribution* explanations are reported in Figure 8. Figures for experiments performed on other distributions are moved to the Appendix under Subsection A.5.

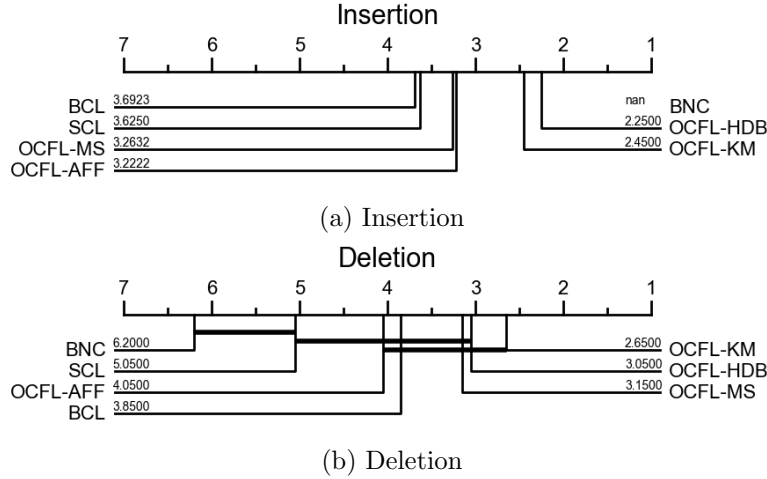


Figure 8: Critical Difference Plots for insertion and deletion. Particular algorithms are ranked and plotted on the x-axis according to the mean AUC value of insertion. The bold black bar indicates that no statistical differences were detected. The plots presents results obtained on the in-distribution sample for the cluster hypothesis function as explained in Algorithm 2.

12. Given an example, assume that INDE scores were calculated for each cluster  $C_i \in C$  following Algorithm 17. Afterwards, a mean value for each of those clusters is calculated, *i.e.*,  $\hat{C}_i = \frac{1}{|C_i|} \sum_{e \in C_i} AUC(e)$ . As the last step, those values are averaged across the clusters, so each run can be represented by a single statistic.

## 6 Scope and limitations

In this Section, we discuss some of the additional considerations and limitations not addressed in the main body of the paper. In Subsection 6.1 we extend our remarks towards privacy issues that were not main part of the considerations under this paper. In Subsection 6.2 we elaborate on the dynamic client environment, where the learning cohort is not stable over the whole training process. Finally, Subsection 6.3 elaborates on the possible extension of the Temperature Function and how the moving average calculated over the last  $N$  round can be used instead of a one-iteration switch implemented in the algorithm presented in this paper.

### 6.1 Privacy Issues

FL was proven to reduce the severity of unintended memorisation, thus reducing the potential data leakage from aggregated models, as proven by Thakkar et al. (2021). However, the baseline version of FL is still vulnerable to privacy breaches, such as Membership Inference Attacks (MIA, see Zhu et al. (2024)), Reconstruction Attacks (RA, see Wang et al. (2023)), and Cross-Silo Mitigation (CSM, see Fontana et al. (2021)). There are several strategies to mitigate those vulnerabilities, including Differential Privacy (DP), which is well studied in the context of the FL (see studies conducted by Wei et al. (2020)). It must be noted that the privacy-related issues were not a primary concern of this work, as we have focused our studies on the personalisation issues and explanation of the knowledge transfer with an additional usage of saliency maps. However, the subsequent studies should focus on that particular problem, addressing issues such as the impact of personalisation on the susceptibility to privacy risks and the cluster-level privacy budgets.

Undoubtedly, the baseline FL offers stronger privacy guarantees by the very fact that the data is kept on the side of local devices. However, those guarantees may not be sufficient, given the nature of the data. It must be noted that our algorithm naturally extends to a majority of privacy-enhancing techniques such as DP, as we do not execute any additional process on the client side nor aggregate any information other than gradients. Although the performance is expected to drop, DP can be easily applied to our method.

On the final note, there is also a trade-off between the personalisation degree and the attack vulnerability. It was proven by Long et al. (2018) that well-generalised models are less vulnerable when it comes to certain types of privacy attacks. One of the advantages of proper clustering is the ability to create a correct clustering structure without creating a situation where some clients are singled out to a separate cluster. Such singled-out clusters can create a substantial privacy risk, as they train models that overfit a particular distribution.

### 6.2 Dynamic Client Environment

The FL paradigm was designed to be dynamic, with clients joining and dropping out of the training at random intervals. In this paper, we have focused on a stable environment where all the clients are sampled each round. Since we use three different benchmark lines (baseline, Sattler et al. (2021) and Briggs et al. (2020)), we wanted to keep the environment stable, so as to receive comparable and unbiased results. However, our algorithm naturally



extends to a dynamic client environment, where One-Shot Clustering is performed on only a subset of clients. Depending on the chosen clustering algorithm, the subsequent client attribution will differ, but in most cases, it will rely on attributing each client to the most appropriate cluster by comparing the received gradients with the given clustering structure. Depending on the ratio of the sample size to the population size, One-Shot Clustering can be turned into Few-Shots Clustering, where the clustering is performed a few times, each time updating the centroids or other appropriate clustering structure.

Similarly to the works of Briggs et al. (2020) and Sattler et al. (2021) that we use as a comparison, we started from the stable federated scenario to briefly extend it into a dynamic environment. Undeniably, clustering is more sensible in a stable environment when there is a clear advantage of establishing a correct division between the sample space. However, we wanted to extend this work with a notion of dynamic clustering to make it complete and set new directions for the research.

### 6.3 Combining Temperature Function with Moving Average

The presented Algorithm 1 assumes performing clustering at the first sign of temperature rise (line 20 of Algorithm 1). Such a use of the Temperature Function was defined at the beginning of our experiments, and given the positive outcome of the experiments, we have decided to present it in this paper. However, a note must be made that it is possible to observe a moving average of the Temperature Function, possibly postponing the clustering in time until we record the divergence of federated gradients is observed throughout several rounds. In such a case, Algorithm 1 will constitute a special case of the presented algorithm, with a time window equal to one. For testing the efficiency of this and other similar methods, we have specially implemented and attached a small prototypical library to this paper, which should allow the reader to experiment with different methods of detecting a suitable moment for performing clustering.

Given the recorded Temperature presented in Section 4.5, we note that employment of the moving average may be even more beneficial to the clustering performance than the switch condition as presented originally. The switch condition (line 20 of Algorithm 1) works well if the Temperature Function exhibits empirical behaviour as presented in Figure 4. However, although this behaviour can be expected on average, individual inspection of runs recorded on particular datasets (Figure 3) clearly indicates that the depending on the model size, chosen hyperparameters, posed learning task, and other factors unaccounted for here, the function may exhibit slightly different patterns. In those cases, the dynamic monitor of the Temperature would be more robust than the static switch condition presented in Algorithm 1. However, as the possible implementations of such a monitoring (for example, with a help of a moving average) are to be considered a special case of the algorithm presented here, we leave it as one of the possible limitations or further research directions.

## 7 Conclusions

In this paper, we have presented a family of OCFL clustering agnostic algorithms that are suitable for performing the split of population at an early stage in an automatic manner. Moreover, by an extensive empirical evaluation over five different datasets, each one in 8 different configurations, we have evidenced the efficiency of the proposed solution, especially

when combined with density-based clustering (i.e. OCFL-MS or OCFL-HDB). Proposed algorithms are able to correctly identify the correct structure of data-generating distributions and attribute clients to an appropriate cluster as early as the first three rounds of the FL process. This has a direct impact on the personalisation of local models, as evidenced by the empirical results.

Moreover, by using saliency maps to inspect local explanations generated by personalised clusters, we were not only able to empirically prove that our solution can deliver better personalisation, but also that the local hypothesis functions are thus able to generate more meaningful explanations on the provided data samples. The intersection of personalisation and (local) explainability in CFL is still a largely unexplored area, with our work - to the best of our knowledge - being the first one that tries to tackle this issue. Due to this, we have not only proven some additional empirical properties of the presented algorithm, but also proposed a few methodological frameworks which can be used to further develop the intersection of those two domains.

## Acknowledgments and Disclosure of Funding

This work was supported by the European Union in projects **LeADS** (GA no. 956562) and **CREXDATA** (GA no. 101092749), NextGenerationEU programme under the funding schemes PNRR-PE-AI scheme (M4C2, investment 1.3, line on AI) FAIR (Future Artificial Intelligence Research), NextGenerationEU – National Recovery and Resilience Plan (Piano Nazionale di Ripresa e Resilienza, PNRR) – Project: “SoBigData.it – Strengthening the Italian RI for Social Mining and Big Data Analytics” – Prot. IR0000013 – Avviso n. 3264 del 28/12/2021”. This work was also funded by the European Union under Grant Agreement no. 101120763 - TANGO. Views and opinions expressed are, however, those of the author(s) only and do not necessarily reflect those of the European Union or the European Health and Digital Executive Agency (HaDEA). Neither the European Union nor the granting authority can be held responsible for them.

## Appendix A.

### A.1 Hyperparameters Set

The Table 3 presents a hyperparameter choice employed for solving classification tasks on particular datasets. In every case, the number of local iterations was always equal to 3 and the general Learning Rate for the FedOPT algorithm was equal to 1.0. Betas are defined as coefficients used for computing running averages of gradient and its square and are applicable only in the case of Adam optimiser. EPS is defined as the term added to the denominator to improve numerical stability and is also defined only for Adam.

DATASET	OPTIMISER	BATCH SIZE	LR	WEIGHT DECAY	BETAS	EPS	GLOBAL ITERATIONS
MNIST	SGD	32	1e-2	0	NA	NA	50
FMNIST	SGD	32	1e-2	0	NA	NA	50
CIFAR10	SGD	64	1e-2	0	NA	NA	80
PATHMNIST	ADAM	128	1e-7	1e-2	(0.9, 0.999)	1e-8	75
BLOODMNIST	ADAM	128	1e-6	1e-2	(0.9, 0.999)	1e-8	75

Table 3: Table presenting the hyperparameters used for solving classification tasks on particular datasets shared for all simulations presented in the paper.

### A.2 Model-Agnostic Distributed Multitask Optimisation Fine-Tuning

The following subsection overviews fine-tuning performed in relation to the Clustered Federated Learning: Model-Agnostic Distributed Multitask Optimisation Under Privacy Constraints presented in the paper of Sattler et al. (2021).

Since the authors’ implementation included in the GitHub repository contained an additional hyperparameter - a minimal number of rounds after which clustering can be performed - we have also transferred that hyperparameter into our implementation. Given that the algorithm of Sattler et al. (2021) requires three hyperparameters (including the cool-down period that is incorporated in the code presented on GitHub), the original authors’ recommendations were employed to select a set of the best hyperparameters for a fair comparison.

As indicated in Subsection 4.2, one problem that connected to that is that authors of Sattler et al. (2021) recommend setting the values of epsilons as  $\epsilon_1 = \max_t \|\Delta\theta_c^t\|/10$  and  $\epsilon_2 \in [\epsilon_1, 10\epsilon_1]$  where  $\Delta\theta_i^t = \text{SGD}(\theta^{t-1}, D_i) - \theta^{t-1}$ . This would require running all the simulation splits, registering the magnitude of gradients, observing the maximal possible magnitude and then choosing that value as a hyperparameter for another run, while also adjusting the cool-down round that was mentioned before. Given the number of simulations performed for the presented studies, this would yield a highly impractical workflow. Moreover, we have noticed that in the original implementation placed in the GitHub repository, the authors also do not construct their experiments in such a way, providing specified  $\epsilon_1$  and  $\epsilon_2$  values from the beginning.

Because of that, an approximation method was constructed for both values. We have performed a centralised training on an original dataset and defined a proxy value  $\Delta\hat{\theta}^t = |\text{SGD}(\theta^t, D) - \text{SGD}(\theta^{t-1}, D)|$  that is used in exchange for the original  $\theta$  value. Afterwards, the round of convergence is used to select the value for a cool-down period. The recommendations from Sattler et al. (2021) are used to select values of  $\epsilon_1$  and  $\epsilon_2$ . The registered  $\epsilon_1$

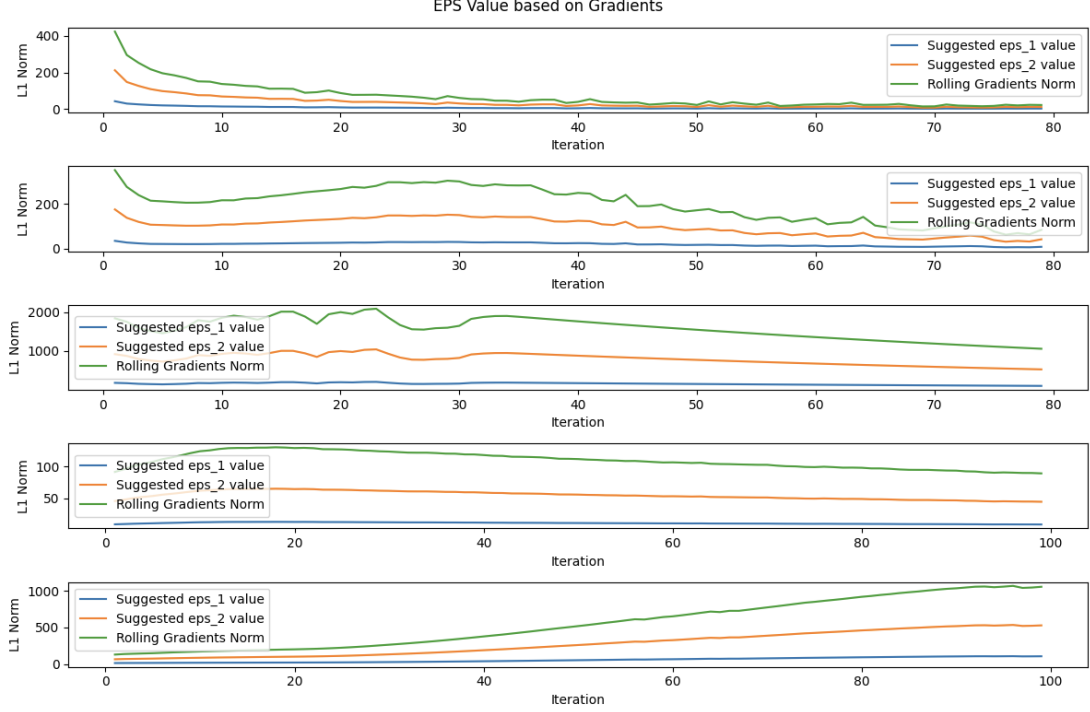


Figure 9: Presentation of the proxy value  $\Delta\hat{\theta}^t = |SGD(\theta^t, D) - SGD(\theta^{t-1}, D)|$  that is used in exchange the approximate the possible  $\theta$  value used in Sattler et al. (2021) as a variable for establishing the approximate values of  $\epsilon_1$  and  $\epsilon_2$  - two hyperparameters that are necessary for a correct clustering performed by the algorithm.

DATASET	$\epsilon_1$	$\epsilon_2$	$c$
MNIST	0.35	1.00	30
FMNIST	0.35	1.00	40
CIFAR10	185.00	925.00	20
PATHMNIST	12	60	40
BLOODMNIST	38	188	40

Table 4: Set of hyperparameters used for Model-Agnostic Distributed Multitask Optimisation presented in Sattler et al. (2021). Sattler’s et al. published values:  $\epsilon_1 = 6.00$  and  $\epsilon_2 = 30.00$  for MNIST and  $\epsilon_1 = 25.00$  and  $\epsilon_2 = 125.00$ .

and  $\epsilon_2$  values on centralised models are presented in Figure 9. Since no recommendations on the clustering round  $c$  were provided in the original paper, we deduced that it must be somehow related to the convergence of the gradients. Hence, we used that heuristic to select an appropriate clustering round  $c$ .

If that failed, we turned to a heuristic search based on the code made available by Sattler et al. (2021). In that way, it was established that one workable combination for MNIST and FMNIST datasets is  $\epsilon_1 = 0.35$  and  $\epsilon_2 = 1.00$ . No such combination was found for CIFAR10 and PathMNIST or BloodMNIST datasets. The set of hyperparameters used specifically for each dataset is reported in Table 4

## A.3 Recorded Value of Temperature Function per Dataset-Datasplit

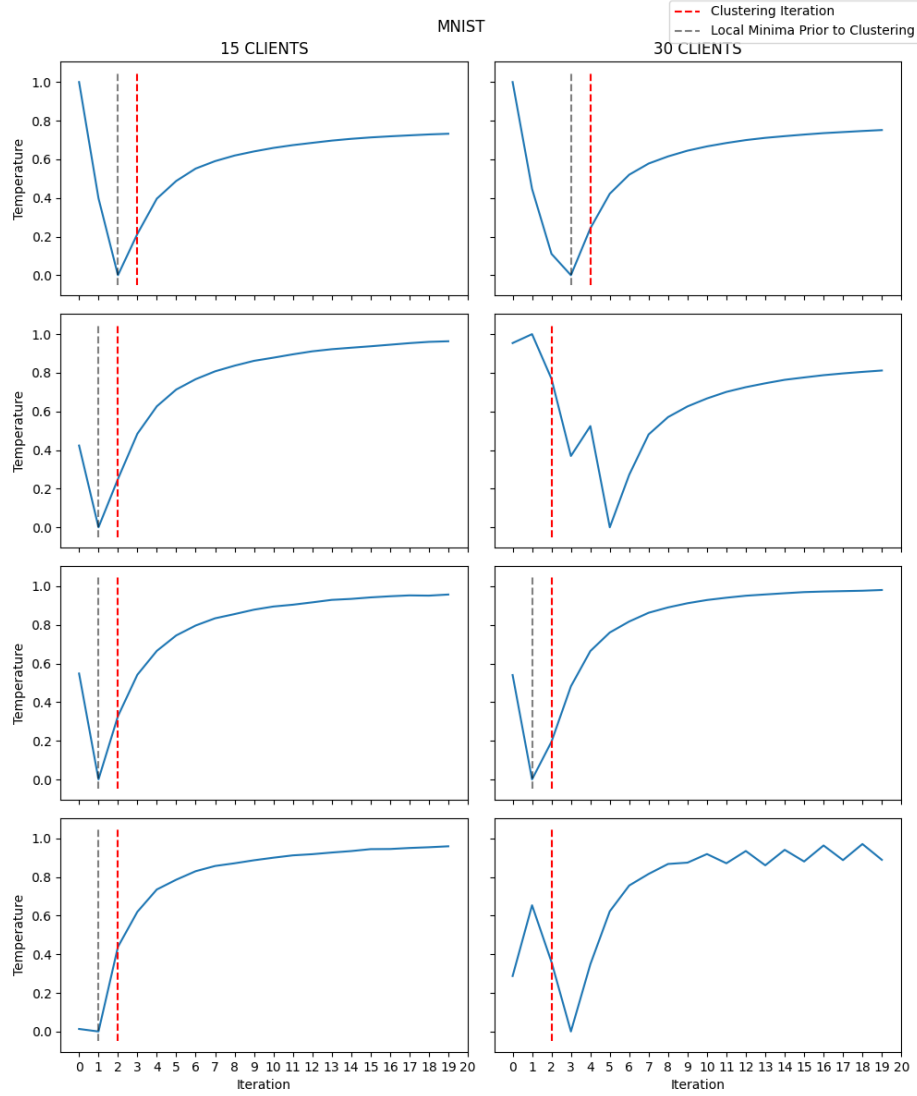


Figure 10: Plots of the (normalised) Temperature Function defined in Definition 7 for the MNIST dataset. Iterations are placed on the y-axis, while the value of the monitored function is placed on the x-axis. Clustering iteration is indicated by a red dotted line, and a local minimum before clustering is indicated by a grey dotted line. Sometimes, the local minimum before clustering does not occur. In that case, only a clustering iteration is plotted on the graph.

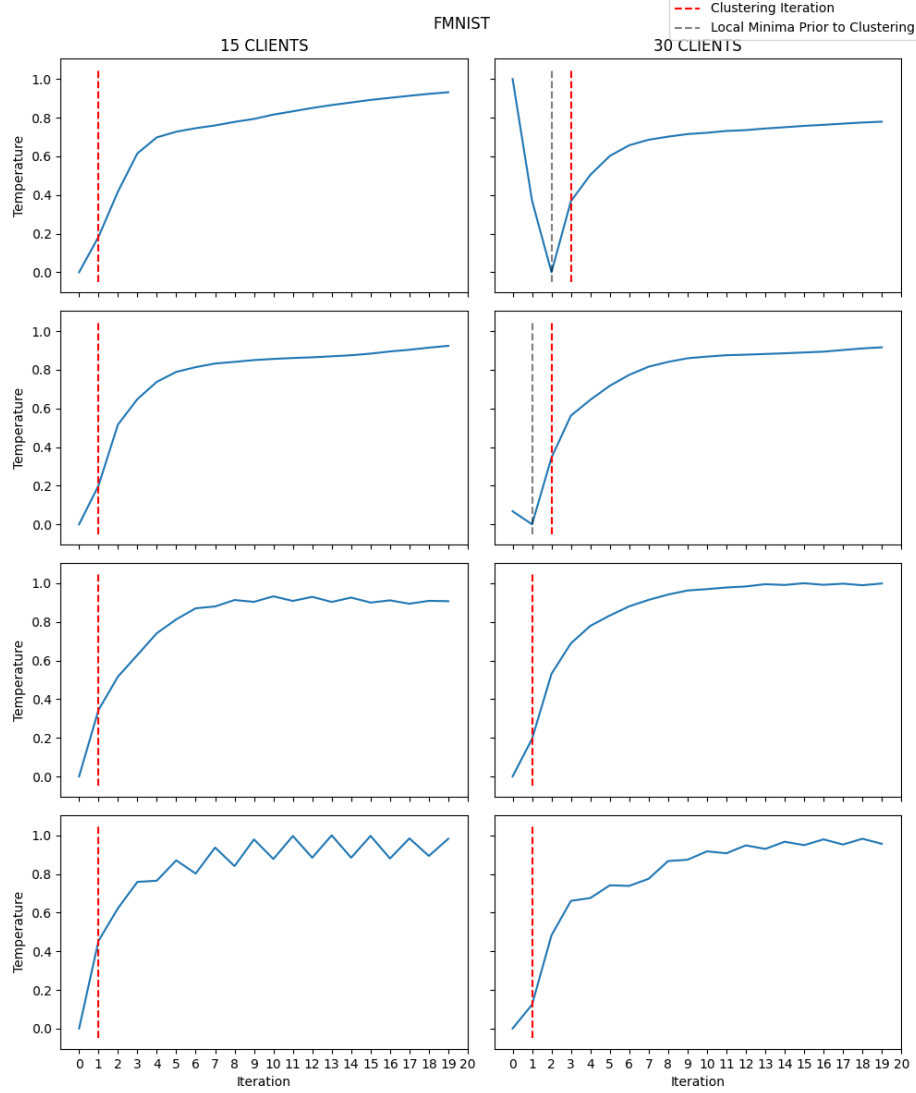


Figure 11: Plots of the (normalised) Temperature Function defined in Definition 7 for the FMNIST dataset. Iterations are placed on the y-axis, while the value of the monitored function is placed on the x-axis. Clustering iteration is indicated by a red dotted line, and a local minimum before clustering is indicated by a grey dotted line. Sometimes, the local minimum before clustering does not occur. In that case, only a clustering iteration is plotted on the graph.

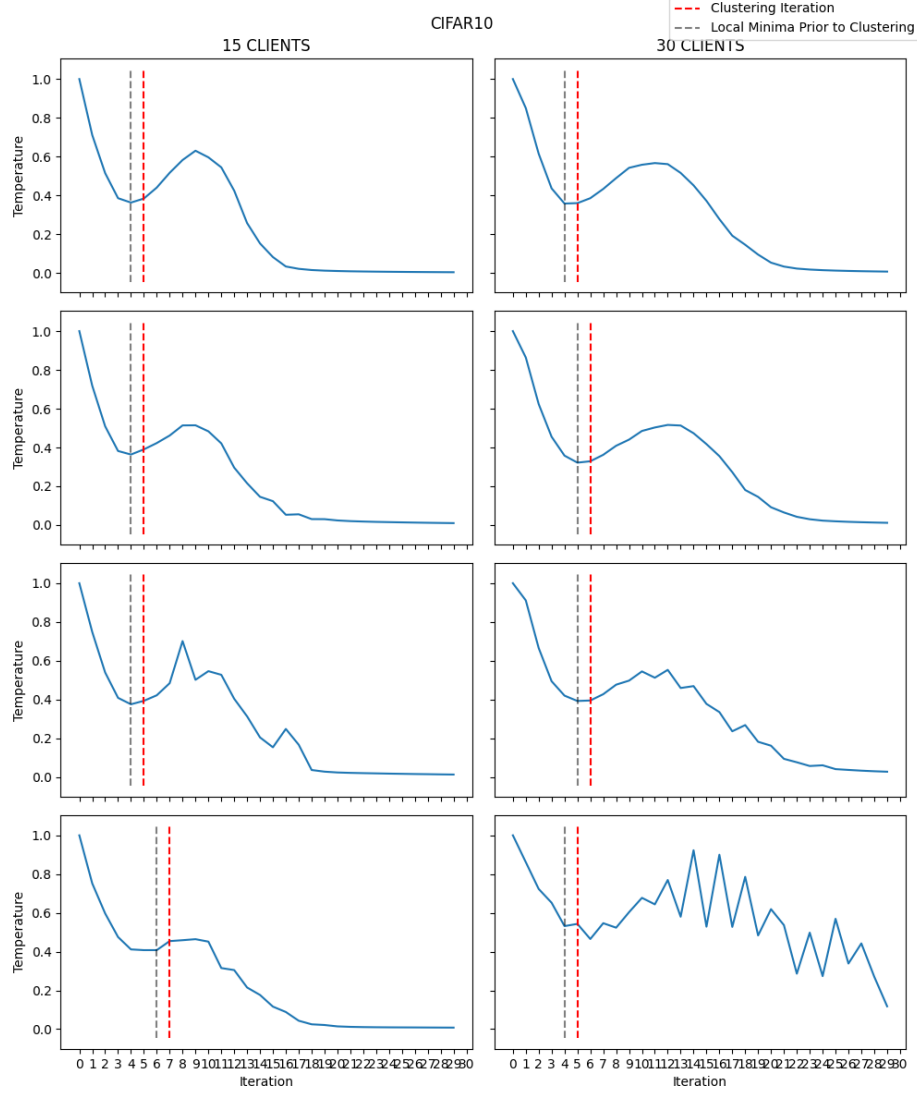


Figure 12: Plots of the (normalised) Temperature Function defined in Definition 7 for the CIFAR10 dataset. Iterations are placed on the y-axis, while the value of the monitored function is placed on the x-axis. Clustering iteration is indicated by a red dotted line, and a local minimum before clustering is indicated by a grey dotted line. Sometimes, the local minimum before clustering does not occur. In that case, only a clustering iteration is plotted on the graph.

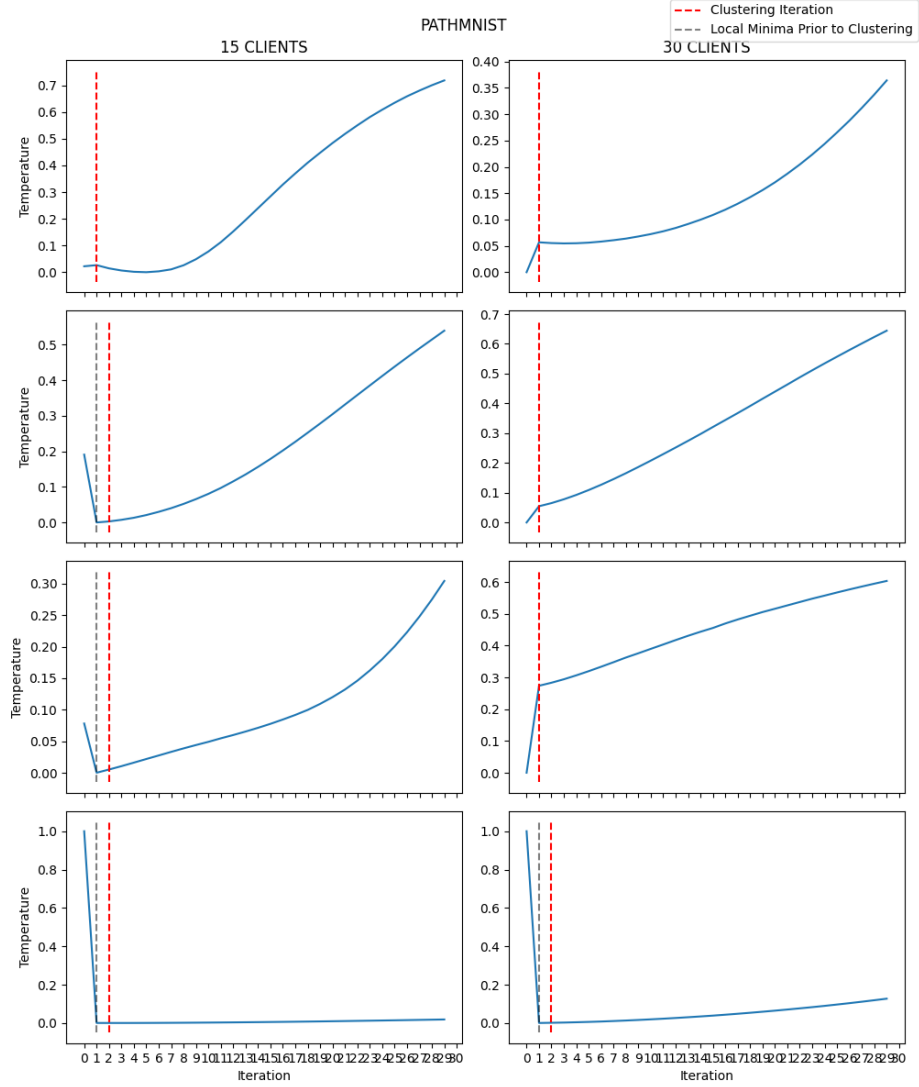


Figure 13: Plots of the (normalised) Temperature Function defined in Definition 7 for the PathMNIST dataset. Iterations are placed on the y-axis, while the value of the monitored function is placed on the x-axis. Clustering iteration is indicated by a red dotted line, and a local minimum before clustering is indicated by a grey dotted line. Sometimes, the local minimum before clustering does not occur. In that case, only a clustering iteration is plotted on the graph.



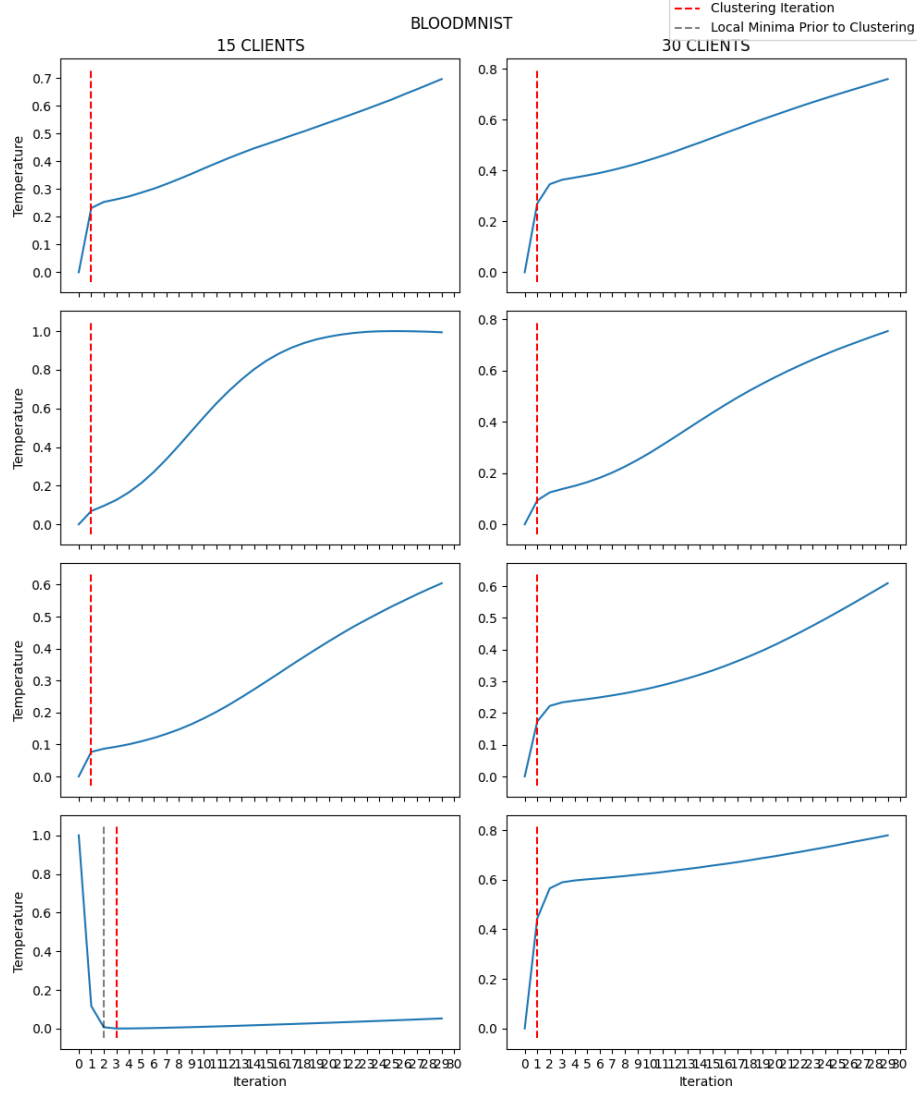


Figure 14: Plots of the (normalised) Temperature Function defined in Definition 7 for the BloodMNIST dataset. Iterations are placed on the y-axis, while the value of the monitored function is placed on the x-axis. Clustering iteration is indicated by a red dotted line, and a local minimum before clustering is indicated by a grey dotted line. Sometimes, the local minimum before clustering does not occur. In that case, only a clustering iteration is plotted on the graph.

## A.4 Demonstration of Individual Saliency Maps

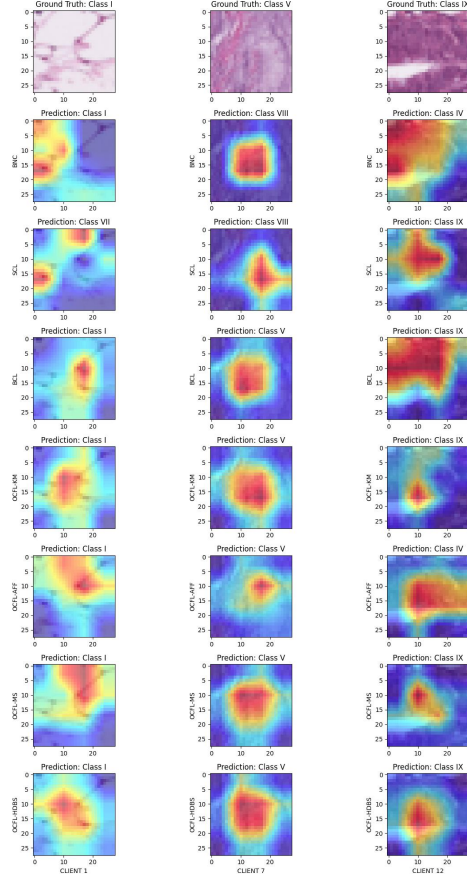


Figure 15: Showcase of various saliency maps generated using seven different local models trained by various clustering algorithms on a PathMNIST dataset: Baseline (BNC), Sattler et al. (2021) (SCL), Briggs et al. (2020) (BCL), OCFL with K-Means (OCFL-KM), OCFL with Affinity (OCFL-AFF), OCFL with MeanShift (OCFL-MS) and OCFL with HDBSCAN (OCFL-HDBS). Each column represents a different client, while each row represents a different clustering algorithm. Additionally, the true and predicted classes are placed above the images.

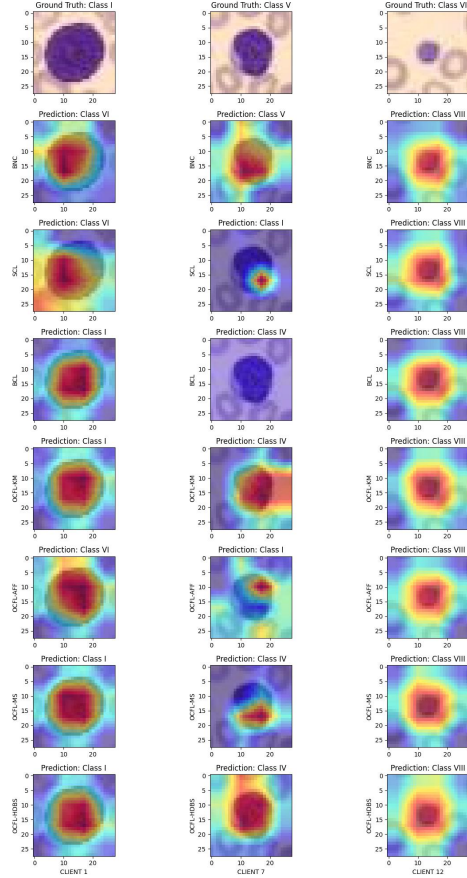


Figure 16: Showcase of various saliency maps generated using seven different local models trained by various clustering algorithms on a BloodMNIST dataset: Baseline (BNC), Sattler et al. (2021) (SCL), Briggs et al. (2020) (BCL), OCFL with K-Means (OCFL-KM), OCFL with Affinity (OCFL-AFF), OCFL with MeanShift (OCFL-MS) and OCFL with HDBSCAN (OCFL-HDBS). Each column represents a different client, while each row represents a different clustering algorithm. Additionally, the true and predicted classes are placed above the images.

### A.5 CD Plots for Insertion-Deletion

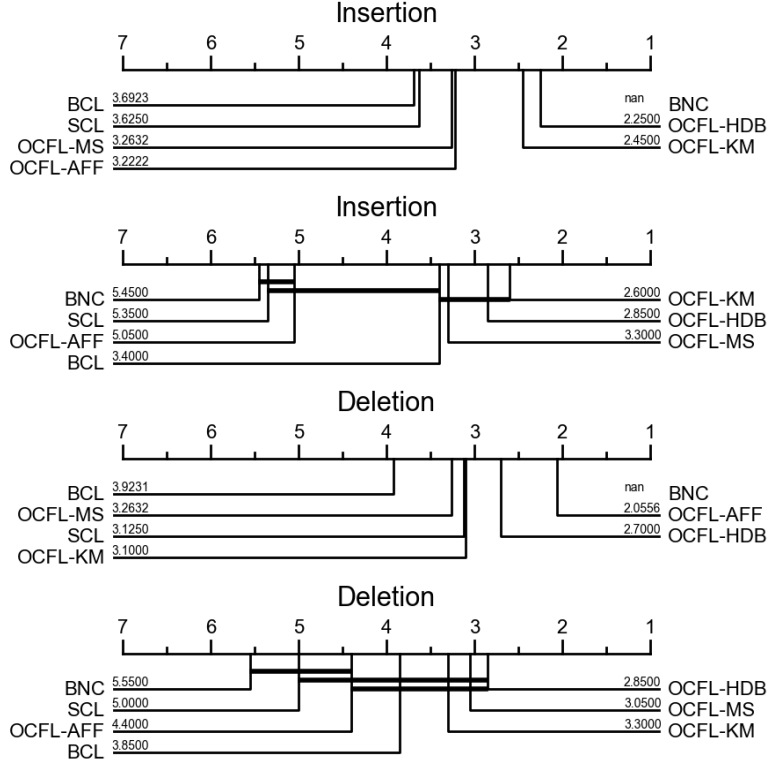


Figure 17: Critical Difference Plots for insertion and deletion. Particular algorithms are ranked and plotted on the x-axis according to the mean AUC value of insertion. The bold black bar indicates that no statistical differences were detected. The plots presents results obtained on the uut-of-cluster sample for the cluster hypothesis function as explained in Algorithm 2.

## Appendix B. Online Resources

As part of this paper, we share an extensive online resource that may help researchers assess the presented One-Shot Clustering Federated Learning (OCFL) algorithm or advance research on the topic of Federated Clustering Learning (FCL) itself.

There are two separate GitHub repositories associated with this paper. The first one contains results obtained during original runs, and the code for generating all the figures. The second one contains code for recreating all the experiments as well as source code for experimenting with modified versions of the presented algorithms. We justify the decision to split the code into two distinct repositories by the fact that the second one contains adjustable code for designing custom experiments. It may be the case that some readers are interested in only one of those repositories; in such a case, it is a better choice to keep them separate.

The repository for all the numerical results can be accessed under the following link. It contains all the numerical results obtained during all the different 280 simulation runs, including a complete set of metrics registered on each client. It also contains a source code for analysing the results and generating graphs and tables presented in this paper. The second repository can be found under the following link. It contains the scripts necessary to reproduce all the simulations. It is also structured in such a way that it is entirely possible to either adjust the hyperparameters of the run (including the clustering algorithm) or the source code itself, making it a perfect boilerplate for further experimentation with the CFL.

## References

- C. Briggs, Z. Fan, and P. Andras. Federated learning with hierarchical clustering of local updates to improve training on non-iid data. In *IJCNN*, pages 1–9. IEEE, 2020.
- D. Comaniciu and P. Meer. Mean shift: A robust approach toward feature space analysis. *IEEE Trans. Pattern Anal. Mach. Intell.*, 24(5):603–619, 2002.
- J. Demsar. Statistical comparisons of classifiers over multiple data sets. *J. Mach. Learn. Res.*, 7:1–30, 2006. URL <https://jmlr.org/papers/v7/demsar06a.html>.
- M. Duan, D. Liu, X. Ji, R. Liu, L. Liang, X. Chen, and Y. Tan. Fed-group: Efficient federated learning via decomposed similarity-based clustering. In *ISPA/BDCloud/SocialCom/SustainCom*, pages 228–237. IEEE, 2021.
- R. C. Fong and A. Vedaldi. Interpretable Explanations of Black Boxes by Meaningful Perturbation. In *2017 IEEE International Conference on Computer Vision (ICCV)*, pages 3449–3457, Oct. 2017. doi: 10.1109/ICCV.2017.371. URL <https://ieeexplore.ieee.org/document/8237633>. ISSN: 2380-7504.
- M. Fontana, F. Naretto, and A. Monreale. A new approach for cross-silo federated learning and its privacy risks. In *PST*, pages 1–10. IEEE, 2021.
- B. J. Frey and D. Dueck. Clustering by Passing Messages Between Data Points. *Science*, 315(5814):972–976, 2007.
- A. Ghosh, J. Chung, D. Yin, and K. Ramchandran. An efficient framework for clustered federated learning. *IEEE Trans. Inf. Theory*, 68(12):8076–8091, 2022.
- B. Gong, T. Xing, Z. Liu, J. Wang, and X. Liu. Adaptive clustered federated learning for heterogeneous data in edge computing. *Mob. Networks Appl.*, 27(4):1520–1530, 2022a.
- B. Gong, T. Xing, Z. Liu, W. Xi, and X. Chen. Adaptive client clustering for efficient federated learning over non-iid and imbalanced data. *IEEE Transactions on Big Data*, pages 1–1, 2022b. doi: 10.1109/TBDATA.2022.3167994.
- K. He, X. Zhang, S. Ren, and J. Sun. Deep residual learning for image recognition. In *CVPR*, pages 770–778. IEEE Computer Society, 2016.

- P. Kairouz, H. B. McMahan, B. Avent, A. Bellet, M. Bennis, A. N. Bhagoji, K. A. Bonawitz, Z. Charles, G. Cormode, R. Cummings, R. G. L. D'Oliveira, H. Eichner, S. E. Rouayheb, D. Evans, J. Gardner, Z. Garrett, A. Gascón, B. Ghazi, P. B. Gibbons, M. Gruteser, Z. Harchaoui, C. He, L. He, Z. Huo, B. Hutchinson, J. Hsu, M. Jaggi, T. Javidi, G. Joshi, M. Khodak, J. Konečný, A. Korolova, F. Koushanfar, S. Koyejo, T. Lepoint, Y. Liu, P. Mittal, M. Mohri, R. Nock, A. Özgür, R. Pagh, H. Qi, D. Ramage, R. Raskar, M. Raykova, D. Song, W. Song, S. U. Stich, Z. Sun, A. T. Suresh, F. Tramèr, P. Vepakomma, J. Wang, L. Xiong, Z. Xu, Q. Yang, F. X. Yu, H. Yu, and S. Zhao. Advances and open problems in federated learning. *Found. Trends Mach. Learn.*, 14(1-2): 1–210, 2021.
- S. P. Karimireddy, S. Kale, M. Mohri, S. J. Reddi, S. U. Stich, and A. T. Suresh. SCAF-FOLD: stochastic controlled averaging for federated learning. In *ICML*, volume 119 of *Proceedings of Machine Learning Research*, pages 5132–5143. PMLR, 2020.
- P. Kindermans, S. Hooker, J. Adebayo, M. Alber, K. T. Schütt, S. Dähne, D. Erhan, and B. Kim. The (un)reliability of saliency methods. In W. Samek, G. Montavon, A. Vedaldi, L. K. Hansen, and K. Müller, editors, *Explainable AI: Interpreting, Explaining and Visualizing Deep Learning*, volume 11700 of *Lecture Notes in Computer Science*, pages 267–280. Springer, 2019. doi: 10.1007/978-3-030-28954-6\_14. URL [https://doi.org/10.1007/978-3-030-28954-6\\_14](https://doi.org/10.1007/978-3-030-28954-6_14).
- D. P. Kingma and J. Ba. Adam: A method for stochastic optimization. In Y. Bengio and Y. LeCun, editors, *3rd International Conference on Learning Representations, ICLR 2015, San Diego, CA, USA, May 7-9, 2015, Conference Track Proceedings*, 2015. URL <http://arxiv.org/abs/1412.6980>.
- A. Krizhevsky. Learning multiple layers of features from tiny images. *CoRR*, 2009. URL <https://www.cs.toronto.edu/~kriz/learning-features-2009-TR.pdf>.
- Y. LeCun and C. Cortes. MNIST handwritten digit database. *CoRR*, 2010. URL <http://yann.lecun.com/exdb/mnist/>.
- C. Li, G. Li, and P. K. Varshney. Federated learning with soft clustering. *IEEE Internet Things J.*, 9(10):7773–7782, 2022. doi: 10.1109/JIOT.2021.3113927. URL <https://doi.org/10.1109/JIOT.2021.3113927>.
- T. Li, A. K. Sahu, M. Zaheer, M. Sanjabi, A. Talwalkar, and V. Smith. Federated optimization in heterogeneous networks. In *MLSys*. mlsys.org, 2020.
- Y. Liu, Y. Kang, T. Zou, Y. Pu, Y. He, X. Ye, Y. Ouyang, Y. Zhang, and Q. Yang. Vertical federated learning: Concepts, advances, and challenges. *IEEE Trans. Knowl. Data Eng.*, 36(7):3615–3634, 2024.
- Y. Long, V. Bindschaedler, L. Wang, D. Bu, X. Wang, H. Tang, C. A. Gunter, and K. Chen. Understanding membership inferences on well-generalized learning models. *CoRR*, abs/1802.04889, 2018.

- J. Ma, G. Long, T. Zhou, J. Jiang, and C. Zhang. On the convergence of clustered federated learning. *CoRR*, abs/2202.06187, 2022.
- C. Malzer and M. Baum. A hybrid approach to hierarchical density-based cluster selection. In *MFI*, pages 223–228. IEEE, 2020.
- Y. Mansour, M. Mohri, J. Ro, and A. T. Suresh. Three approaches for personalization with applications to federated learning. *CoRR*, abs/2002.10619, 2020.
- B. McMahan, E. Moore, D. Ramage, S. Hampson, and B. A. y Arcas. Communication-efficient learning of deep networks from decentralized data. In *AISTATS*, volume 54 of *Proceedings of Machine Learning Research*, pages 1273–1282. PMLR, 2017a.
- B. McMahan, E. Moore, D. Ramage, S. Hampson, and B. A. y Arcas. Communication-efficient learning of deep networks from decentralized data. In *AISTATS*, volume 54 of *Proceedings of Machine Learning Research*, pages 1273–1282. PMLR, 2017b.
- Mirko Bunse. CriticalDifferenceDiagrams.jl. URL <https://mirkobunse.github.io/CriticalDifferenceDiagrams.jl/stable/>.
- C. Palihawadana, N. Wiratunga, A. Wijekoon, and H. K. Kalutarage. Fedsim: Similarity guided model aggregation for federated learning. *Neurocomputing*, 483:432–445, 2022.
- V. Petsiuk, A. Das, and K. Saenko. RISE: randomized input sampling for explanation of black-box models. In *British Machine Vision Conference 2018, BMVC 2018, Newcastle, UK, September 3-6, 2018*, page 151. BMVA Press, 2018. URL <http://bmvc2018.org/contents/papers/1064.pdf>.
- S. J. Reddi, Z. Charles, M. Zaheer, Z. Garrett, K. Rush, J. Konečný, S. Kumar, and H. B. McMahan. Adaptive federated optimization. *CoRR*, abs/2003.00295, 2020.
- S. J. Reddi, Z. Charles, M. Zaheer, Z. Garrett, K. Rush, J. Konečný, S. Kumar, and H. B. McMahan. Adaptive federated optimization. In *ICLR*. OpenReview.net, 2021.
- Y. Ruan and C. Joe-Wong. Fedsoft: Soft clustered federated learning with proximal local updating. In *Thirty-Sixth AAAI Conference on Artificial Intelligence, AAAI 2022, Thirty-Fourth Conference on Innovative Applications of Artificial Intelligence, IAAI 2022, The Twelveth Symposium on Educational Advances in Artificial Intelligence, EAAI 2022 Virtual Event, February 22 - March 1, 2022*, pages 8124–8131. AAAI Press, 2022. doi: 10.1609/AAAI.V36I7.20785. URL <https://doi.org/10.1609/aaai.v36i7.20785>.
- S. Z. S. Samuel, V. Kamakshi, N. Lodhi, and N. C. Krishnan. Evaluation of saliency-based explainability method. *CoRR*, abs/2106.12773, 2021. URL <https://arxiv.org/abs/2106.12773>.
- F. Sattler, K. Müller, and W. Samek. Clustered federated learning: Model-agnostic distributed multitask optimization under privacy constraints. *IEEE Trans. Neural Networks Learn. Syst.*, 32(8):3710–3722, 2021.

- K. Simonyan and A. Zisserman. Very deep convolutional networks for large-scale image recognition. In *ICLR*, 2015.
- A. Z. Tan, H. Yu, L. Cui, and Q. Yang. Towards personalized federated learning. *IEEE Trans. Neural Networks Learn. Syst.*, 34(12):9587–9603, 2023. doi: 10.1109/TNNLS.2022.3160699. URL <https://doi.org/10.1109/TNNLS.2022.3160699>.
- O. D. Thakkar, S. Ramaswamy, R. Mathews, and F. Beaufays. Understanding unintended memorization in language models under federated learning. In O. Feyisetan, S. Ghanavati, S. Malmasi, and P. Thaine, editors, *Proceedings of the Third Workshop on Privacy in Natural Language Processing*, pages 1–10, Online, June 2021. Association for Computational Linguistics. doi: 10.18653/v1/2021.privatenlp-1.1. URL <https://aclanthology.org/2021.privatenlp-1.1>.
- P. Tian, W. Liao, W. Yu, and E. Blasch. WSCC: A weight-similarity-based client clustering approach for non-iid federated learning. *IEEE Internet Things J.*, 9(20):20243–20256, 2022.
- J. Wang, Z. Charles, Z. Xu, G. Joshi, H. B. McMahan, B. A. y Arcas, M. Al-Shedivat, G. Andrew, S. Avestimehr, K. Daly, D. Data, S. N. Diggavi, H. Eichner, A. Gadhihar, Z. Garrett, A. M. Girgis, F. Hanzely, A. Hard, C. He, S. Horváth, Z. Huo, A. Ingerman, M. Jaggi, T. Javidi, P. Kairouz, S. Kale, S. P. Karimireddy, J. Konečný, S. Koyejo, T. Li, L. Liu, M. Mohri, H. Qi, S. J. Reddi, P. Richtárik, K. Singhal, V. Smith, M. Soltanolkotabi, W. Song, A. T. Suresh, S. U. Stich, A. Talwalkar, H. Wang, B. E. Woodworth, S. Wu, F. X. Yu, H. Yuan, M. Zaheer, M. Zhang, T. Zhang, C. Zheng, C. Zhu, and W. Zhu. A field guide to federated optimization. *CoRR*, abs/2107.06917, 2021.
- Z. Wang, Y. Song, and E. Zuazua. Approximate and weighted data reconstruction attack in federated learning. *CoRR*, abs/2308.06822, 2023.
- K. Wei, J. Li, M. Ding, C. Ma, H. H. Yang, F. Farokhi, S. Jin, T. Q. S. Quek, and H. V. Poor. Federated learning with differential privacy: Algorithms and performance analysis. *IEEE Trans. Inf. Forensics Secur.*, 15:3454–3469, 2020.
- H. Xiao, K. Rasul, and R. Vollgraf. Fashion-mnist: a novel image dataset for benchmarking machine learning algorithms. *CoRR*, abs/1708.07747, 2017.
- J. Yang, R. Shi, D. Wei, Z. Liu, L. Zhao, B. Ke, H. Pfister, and B. Ni. Medmnist v2-a large-scale lightweight benchmark for 2d and 3d biomedical image classification. *Scientific Data*, 10(1):41, 2023.
- G. Zhu, D. Li, H. Gu, Y. Han, Y. Yao, L. Fan, and Q. Yang. Evaluating membership inference attacks and defenses in federated learning. *CoRR*, abs/2402.06289, 2024.